J. Fluid Mech. (2002), *vol.* 468, *pp.* 283–315.
DOI: 10.1017/S0022112002001738 Printed in the United Kingdom

Mechanisms for particle transfer and segregation in a turbulent boundary layer

By CRISTIAN MARCHIOLI AND ALFREDO SOLDATI†

Centro Interdipartimentale di Fluidodinamica e Idraulica and Dipartimento di Scienze e Tecnologie Chimiche, Università di Udine, Udine, 33100, Italy

(Received 2 August 2001 and in revised form 20 May 2002)

Particle transfer in the wall region of turbulent boundary layers is dominated by the coherent structures which control the turbulence regeneration cycle. Coherent structures bring particles toward and away from the wall and favour particle segregation in the viscous region, giving rise to non-uniform particle distribution profiles which peak close to the wall. The object of this work is to understand the reasons for higher particle concentration in the wall region by examining turbulent transfer of heavy particles to and away from the wall in connection with the coherent structures of the boundary layer. We will examine the behaviour of a dilute dispersion of heavy particles – flyashes in air – in a vertical channel flow, using pseudo-spectral direct numerical simulation to calculate the turbulent flow field at a shear Reynolds number $Re_\tau = 150$, and Lagrangian tracking to describe the dynamics of particles. Drag force, gravity and Saffman lift are used in the equation of motion for the particles, which are assumed to have no influence on the flow field. Particle interaction with the wall is fully elastic. As reported in several previous investigations, we found that particles are transferred by sweeps – Q2 type events – in the wall region, where they preferentially accumulate in the low-speed streak environments, whereas ejections – Q4 type events – transfer particles from the wall region to the outer flow. We quantify the efficiency of the instantaneous realizations of the Reynolds stresses events in transferring different size particles to the wall and away from the wall, respectively. Our findings confirm that sweeps and ejections are efficient transfer mechanisms for particles. In particular, we find that only those sweep and ejection events with substantial spatial coherence are effective in transferring particles. However, the efficiency of the transfer mechanisms is conditioned by the presence of particles to be transferred. In the case of ejections, particles are more rarely available since, when in the viscous wall layer, they are concentrated under the low-speed streaks. Even though the low-speed streaks are ejection-like environments, particles remain trapped for a long time. This phenomenon, which causes accumulation of particles in the near-wall region, can be interpreted in terms of overall fluxes toward and away from the wall by the theory of turbophoresis. This theory, proposed initially by Caporaloni *et al.* (1975) and re-examined later by Reeks (1983), can help to explain the existence of net particle fluxes toward the wall as a manifestation of the skewness in the velocity distribution of the particles (Reeks 1983). To understand the local and instantaneous mechanisms which give rise to the phenomenon of turbophoresis, we focus on the near-wall region of the turbulent boundary layer. We examine the role of the rear-end of a quasi-streamwise vortex very near to the wall in preventing particles in the proximity of the wall from being re-entrained by the pumping action of the large, farther from the wall, forward-end of a following quasi-streamwise vortex. We examine several mechanisms

† Author to whom correspondence should be addressed: soldati@uniud.it

for turbulence structures near the wall and we find that the mechanism based on the archetypal quasi-streamwise structures identified by Schoppa & Hussain (1997), the parent–offspring regeneration cycle for near-wall quasi-streamwise vortices discussed by Brooke & Hanratty (1993), and the mechanism based on coherent packets of hairpin vortices, the fundamental super-structure characterized by Adrian, Meinhart & Tomkins (2000), all depict the same characteristic pattern which is responsible for particle trapping very near to the wall.

1. Introduction

The physics of particle transfer in a turbulent boundary layer is of great importance in a number of applications, from environmental systems to industrial processes. Turbulent particle transfer mechanisms in the proximity of a wall are characterized by complex interactions between turbulence structures and the dispersed phase. Despite several decades of extensive experimental and numerical studies (Friedlander & Johnstone 1957), exhaustive explanations of particle transfer mechanisms have still to be produced. For instance, it is widely accepted that heavy particles have a tendency to migrate toward the wall (Caporaloni *et al.* 1975; Reeks 1983; McLaughlin 1989; Brooke *et al.* 1992) and that, when in the wall layer, they segregate preferentially in regions characterized by streamwise velocity lower than the mean (Pedinotti, Mariotti & Banerjee 1992; Eaton & Fessler 1994; Niño & García 1996; Pan & Banerjee 1996), and yet explanations which offer physical mechanisms to justify and, possibly, link these observations appear incomplete.

The answer to particle behaviour in turbulent boundary layer is to be found in the relationships between turbulence structures and particle dynamics. This will explain the relationship between turbulence structure and particle number density (Rouson & Eaton 2001), which is the relevant information sought, and it could suggest ways to size and control transfer rates, mixing processes and reaction rates.

A brief literature review will help to clarify some of the currently open issues on particle behaviour in turbulent boundary layers.

Cleaver & Yates (1975) proposed a sublayer model for the deposition of small solid particles from a turbulent gas stream, which emphasizes the role of ejections and sweeps – Q2 and Q4 type events respectively – which are instantaneous realizations of the Reynolds stresses, in determining the deposition rates. Once a particle is entrained in a sweep, i.e. there is fluid downwash toward the wall, it is expected to continue within the sweep and to approach the wall. The possibility of contacting the boundary depends on particle inertia and on the position at which the particle is entrained by the sweep. Only those particles entrained in the sweeps are likely to reach the wall: the others will be under the influence of outward fluid motions which will drive them away from the wall into the outer region. This and several other findings by a number of researchers who reported and demonstrated accumulation of particles close to the wall (Caporaloni *et al.* 1975; Reeks 1983; Sun & Lin 1986; Kallio & Reeks 1989) led to the conclusion that the mechanisms which transfer particles to the wall are more efficient than those which entrain particles into the outer flow.

Since the first detailed direct numerical simulation (DNS) of turbulent channel flow (Kim, Moin & Moser 1987), it has been possible to examine accurately the role of time-dependent turbulence structures in particle behaviour in the boundary

layer. Among the subsequent DNS-driven works, McLaughlin (1989) was the first to exploit a direct simulation of turbulence to simulate a three-dimensional time-dependent vertical channel flow, in which rigid spherical particles were released. The author observed that particles tend to accumulate in the viscous sublayer by virtue of inward turbulent motions in the buffer region, i.e. sweeps. He observed also that particles have a large residence time in the viscous sublayer.

From similar simulations, Brooke *et al.* (1992) found that particles appear to be driven toward the wall by coherent eddies which impart strong spanwise wall-parallel motions to the particle trajectories before they are deposited. These coherent eddies are the same quasi-streamwise structures which play a fundamental role in the wall turbulence regeneration cycle (Guezennec, Piomelli & Kim 1989; Lyons, Hanratty & McLaughlin 1991; Brooke & Hanratty 1993; Schoppa & Hussain 1996, 1997; Jeong *et al.* 1997; Jimenez & Pinelli 1999; Adrian, Meinhart & Tomkins 2000; Soldati & Marchioli 2001) and which control turbulence scalar transfer mechanisms at the wall (De Angelis *et al.* 1997). The mechanism for particle trapping developed by Brooke *et al.* (1992) suggests that particles undergo a long lasting sideways wandering motion in the wall-normal direction until they are trapped in the coherent quasi-streamwise vortex which brings them directly to the wall. In the viscous sublayer, the spanwise motion of this vortex overwhelms the motion toward the wall so that particles experience a wall-parallel transverse drift which acts to concentrate them in low-speed streaks.

This scenario is similar to that proposed by Banerjee and co-workers: their simulations (see Pedinotti *et al.* 1992; Pan & Banerjee 1996) and experiments (Kaftori, Hetsroni & Banerjee 1995*a*, *b*) relative to almost neutrally buoyant inertial particles in horizontal channels, indicate that particle motion, as well as entrainment and deposition processes, are controlled by the action of coherent wall structures. The behaviour of particles is consistent with the motion and the effects of such structures, which appear to have a triple effect: (i) they cause the formation of particle streaks in the low-speed regions near the wall, (ii) they create suitable conditions for particle entrainment and (iii) they assist in deposition, by conveying particles from the outer flow to the wall region through downsweeps, and eventually in particle resuspension, by conveying them from the wall region to the outer flow through ejections. Further analyses on particle fluxes (Kaftori *et al.* 1995*b*) showed that particles which tend to concentrate in low-velocity regions are ascending ones, indicating that the low-velocity environment is preferred by particles with an off-the-wall (rather than downward) trajectory.

Experiments with sand particles in water were performed by García and co-workers (Niño & García 1996; García, Niño & Lopez 1996). They observed that particles located in the viscous layer are effectively re-entrained into the outer flow by intense Q2 type events which occur almost in correspondence with a shear layer which travels near the wall and extends about 100 and 500 wall units in the wall-normal and the streamwise directions respectively (Jimenez *et al.* 1988; Urushihara, Meinhart & Adrian 1993; García, Lopez & Niño 1995). These observations can be explained by the mechanism proposed by Adrian *et al.* (2000). They identify a super-structure composed of a packet of hairpin vortices travelling at the same convection velocity. The fluid region enclosed among the hairpin vortices is a low-velocity region characterized by a series of Q2 events. The strong ejection of wall fluid which occurs at the end of the packet could be the cause of the intense particle re-entrainment observed by Niño & García (1996).

Other recent direct numerical simulations of particle dispersion in turbulent

channel flow (see Ounis, Ahmadi & McLaughlin 1993; Uijttewaal & Oliemans 1996; van Haarlem, Boersma & Nieuwstadt 1998; Rouson & Eaton 2001) and in a three-dimensional mixing layer (Wei Ling *et al.* 1998) confirm that the dynamics of turbulent dispersion phenomena are strongly influenced by coherent wall structures and the related sweep–ejection events cycle.

Despite the general consensus on several features of particle behaviour in the boundary layer, there are still many open issues concerning particle transfer mechanisms and particle segregation. In particular, even though we may safely hypothesize that sweeps and ejections control particle transfer to the wall and away from the wall, it is not entirely clear why particles tend to accumulate at the wall (Young & Leeming 1997; Cerbelli, Giusti & Soldati 2001), or why, once at the wall, particles remain trapped in the low-streamwise-velocity regions at a distance from the wall not exceeding few wall units. In particular, there is puzzling evidence that even though Q2 type events are effective in transferring particles away from the viscous region, when segregated at the wall particles are trapped in the low-speed streaks, which are the signature of Q2 type events. We remark here that preferential concentration of particles in the wall region has been observed in cases in which gravity does not play a role, both in horizontal flows with neutrally buoyant particles (Kaftori *et al.* 1995*b*) and in vertical flows (Uijttewaal & Oliemans 1996; Cerbelli *et al.* 2001). In this work, we will try to address these still unclear issues.

We present results from a direct numerical simulation of the passive transport of solid particles – flyashes – in a fully developed upward turbulent channel flow. Our aim is to identify the role of turbulence structures which are responsible for particle motion and distribution in the buffer region, and which are also responsible for particle entrainment and deposition. We will first try to evaluate from a quantitative point of view the role of sweeps and ejections – i.e. Q2 and Q4 type events. We start from a well-established background on wall turbulence (see Brooke *et al.* 1992; Brooke & Hanratty 1993; Schoppa & Hussain 1996, 1997; Jeong *et al.* 1997; Adrian *et al.* 2000) focusing first on a simplified, though still complex and fully relevant, theoretical case in which the feedback of particles onto the flow field is ignored. Since our calculations involved large swarms of particles – $O(10^5)$ – the one-way coupling allowed us to reduce the computing time required. We believe, nevertheless, that our results are of general validity for dilute dispersions. Previous experiments (Kulick, Fessler & Eaton 1994; Kaftori *et al.* 1995*a*, *b*) demonstrate that turbulence modifications due to the presence of small particles at low enough concentration are negligible. Even though particle concentration in the wall region may be locally large, turbulence structures appear modified only quantitatively – these are only small modifications of the intensities.

In the boundary layer, the most statistically common quasi-streamwise coherent structures are single streamwise-oriented vortices, generally centred within the buffer layer, slightly tilted upward – about 9° average – with streamwise dimension of 200–400 wall units; clockwise and counter-clockwise rotating vortices are also slightly tilted 4° left and right respectively (Schoppa & Hussain 1996, 1997). Quasi-streamwise vortices generate strongly coherent sweeps on the downwash side and strongly coherent ejections on the upwash side.

In the outer region, several recent investigations suggest that the most common vortex structures appear like hairpins whose legs are the counter-rotating quasi-streamwise vortices in the near-wall region (Robinson 1991). These hairpins usually do not possess perfect spanwise symmetry nor do the counter-rotating vortices have equal strength. Spanwise-axisymmetric one-sided hairpins are also observed

(Guezennec & Choi 1989). These new models revise and improve the classical concept of Ω-shaped horseshoe vortices and are widely, though not totally, accepted. In recent papers, Zhou *et al.* (1999) and Adrian *et al.* (2000) proposed a new mechanism for turbulence regeneration cycle which is based on packets of hairpin vortices travelling at the same convection velocity, a new fundamental super-structure. Apparently, these super-structures populate all regions of the turbulent boundary layer and their characteristics fit well with most previous quantitative observations from Kline *et al.* (1967) up to the most recent. Furthermore, Adrian *et al.* (2000) report that if we focus our attention only on the near-wall region – i.e. less than 60 wall units from the wall – the phenomenology of the hairpin packet is very similar to the structures proposed by Schoppa & Hussain (1997) and Jeong *et al.* (1997).

As observed before, particles have a tendency to segregate at the wall in a very thin layer of few wall units (Kaftori *et al.* 1995*b*; Young & Leeming 1997). To explain why particle fluxes away from the wall are not sufficient to ensure a uniform concentration profile we have to look at the behaviour of particles in connection with the dynamics of the structures present very near to the wall.

The purpose of this work is to establish a physical link between the large-scale streamwise structures which populate the wall region and control momentum transfer to the wall and particle transfer fluxes. Further, we will try to provide evidence for the mechanisms which trap particles at the wall.

First, we will establish from a quantitative viewpoint the role of sweeps and ejections in determining particle fluxes to the wall and away from the wall. Second, we will focus on the mechanisms which prevent particles from being entrained by ejections and trap them under the low-speed streaks. In this context, we will examine the role of statistically probable secondary quasi-streamwise vortices, the characteristics of which were described in the context of different theories by Brooke & Hanratty (1993), Bernard, Thomas & Handler (1993), Schoppa & Hussain (1997) and Adrian *et al.* (2000).

2. Numerical simulation

2.1. *Channel flow simulation*

The flow into which particles are introduced is a turbulent channel flow of air, assumed to be incompressible and Newtonian. The flow is driven upward by a pressure gradient. The reference geometry consists of two infinite vertical flat parallel walls: the origin of the coordinate system is located at the centre of the channel and the x-, y- and z-axes point in the streamwise, spanwise and wall-normal directions respectively. Gravity is directed along the negative x-direction. Periodic boundary conditions are imposed on the fluid velocity field in both the streamwise and spanwise directions and no-slip boundary conditions are enforced at the walls. We assume that particle number density and particle size are both small, and that there is no feedback of the particles onto the gas flow.

The flow field was calculated by integrating mass and momentum balance equations in dimensionless form, obtained using the duct half-width, h, and the shear velocity, u_τ, defined as

$$u_\tau = \left(\frac{\tau_w}{\rho}\right)^{1/2}, \tag{2.1}$$

where τ_w is the shear at the wall and ρ is fluid density. Therefore, mass and momentum

balance equations in dimensionless form are

$$\frac{\partial u_i}{\partial x_i} = 0 \tag{2.2}$$

and

$$\frac{\partial u_i}{\partial t} = -u_j \frac{\partial u_i}{\partial x_j} + \frac{1}{Re} \frac{\partial^2 u_i}{\partial x_j \partial x_j} - \frac{\partial p}{\partial x_i} + \delta_{1,i}, \tag{2.3}$$

where u_i is the ith component of the dimensionless velocity vector, p is the fluctuating kinematic pressure (pressure divided by density), $\delta_{1,i}$ is the mean dimensionless pressure gradient that drives the flow, and $Re_\tau = hu_\tau/\nu$ is the shear Reynolds number. Equations (2.2) and (2.3) were solved directly using a pseudo-spectral method previously used in different types of flow (Pan & Banerjee 1996; Soldati & Banerjee 1998) and similar to that used by Kim *et al.* (1987) to solve the turbulent, closed-channel flow problem. Equation (2.3) may be recast as

$$\frac{\partial u_i}{\partial t} = S_i + \frac{1}{Re_\tau} \frac{\partial^2 u_i}{\partial x_j \partial x_j} - \frac{\partial p}{\partial x_i}, \tag{2.4}$$

where S_i includes the convective term and the mean pressure gradient (Kim *et al.* 1987; Lam & Banerjee 1992). The pseudo-spectral method is based on transforming the field variables into wavenumber space, using Fourier representations for the streamwise and spanwise directions and a Chebyshev representation for the wall-normal (non-homogeneous) direction. A two-level explicit Adams–Bashforth scheme for the nonlinear terms S_i and an implicit Crank–Nicolson method for the viscous terms were employed for time advancement. Details of the method have been published previously (Lam & Banerjee 1992).

In the present study, we consider air with density of $1.3\,\mathrm{kg\,m^{-3}}$ and kinematic viscosity of $15.7 \times 10^{-6}\,\mathrm{m^2\,s^{-1}}$. Since the pressure gradient is equal for all simulations, the shear velocity is $11.775 \times 10^{-2}\,\mathrm{m\,s^{-1}}$, and the shear Reynolds number, Re_τ, is equal to 150. The mean velocity is $1.65\,\mathrm{m\,s^{-1}}$ and the Reynolds number based on mean velocity and half duct width is ≈ 2110. Our calculations have been performed in dimensionless units, the Reynolds number being the one parameter to scale the flow. The computational domain was $1885 \times 942 \times 300$ wall units in x, y and z with $64 \times 64 \times 65$ nodes. The spacing of collocation points in the streamwise and spanwise directions was $\Delta x^+ \approx 30$, $\Delta y^+ \approx 15$ in wall units. The first collocation point away from the wall is at $z^+ = 0.18$: this grid resolution is sufficient to describe the significant length scales in the channel flow. The time step used was $\Delta t^+ = 0.35325$ in wall time units. We will not show here the statistics of the flow field which match closely those obtained by Lyons *et al.* (1991) for the same Reynolds number.

Even though the grid is slightly less refined than other DNS databases (Kim *et al.* 1987), the large-scale wall structures are well resolved. We compared the 64^3 results against results obtained with a 128^3 grid (twice the resolution in each direction). From a statistical viewpoint, the results obtained with the two different grids match closely, both collapsing on the results obtained by Lyons *et al.* (1991) for the same Reynolds number. We examined in detail the evolution of the wall structures below $z^+ = 80$. We found hardly any difference in the shape, extent and duration of the structures which dominate wall transfer mechanisms – large-scale quasi-streamwise vortices, low-speed streaks, sweeps and ejections.

An accurate calculation of the forces acting on the particle requires accurate

evaluation of the instantaneous fluid velocity at the particle location. Balachandar & Maxey (1989) used a fourth-order Hermitian scheme in two directions followed by a Fourier interpolation in the third direction. Yeung & Pope (1988) tested both a third-order Taylor-series interpolation scheme and a cubic-spline scheme, concluding that the first scheme gives higher interpolation accuracy with adequate spatial resolution. Pan & Banerjee (1996) used cubic splines as well as a hybrid interpolation scheme that employs cubic-splines in the homogeneous directions followed by a Chebyshev summation in the non-homogeneous direction. This approach is similar to that proposed by Kontomaris, Hanratty & McLaughlin (1992), who employed Lagrange polynomials in the homogeneous directions and Chebyshev polynomials in the non-homogeneous direction. This procedure was found to be highly accurate and the computational work requirement was smaller by roughly the factor $(6/N_x)(6/N_y)$ than the computational work requirement for a fully spectral evaluation of the fluid velocity field at the centre of the particle, which involves summing the Fourier–Chebyshev series (Soldati *et al.* 1997).

In recent papers, several authors who investigated the behaviour of large swarms of particles used time-efficient lower-order interpolation schemes, proving they were accurate enough to maintain statistical accuracy (van Haarlem *et al.* 1998) and to preserve local resolution for the small scales of the boundary layer (Rouson & Eaton 2001). Among the others, Rouson & Eaton (2001) used a three-dimensional linear interpolation, whereas van Haarlem *et al.* (1998) and Uijttewaal & Oliemans (1996) used a quadratic interpolation scheme. In the present work, we used a Lagrange interpolation of order three.

2.2. *Particle equation of motion*

Particles are injected into the flow at concentration low enough for particle–particle interaction due to their inertial force to be negligible – dilute system conditions. Furthermore, particles are assumed to be pointwise, rigid, spherical and to obey the following vectorial Lagrangian equation of motion:

$$\frac{\mathrm{d}\boldsymbol{v}}{\mathrm{d}t} = \frac{C_d}{\tau_P}(\boldsymbol{u}-\boldsymbol{v}) + \left(1-\frac{\rho}{\rho_P}\right)\boldsymbol{g} - \xi(\epsilon)\frac{6.46}{12\pi}\frac{d_P}{\tau_P}\left|\frac{\partial u_x}{\partial z}\right|^{1/2}(v_x-u_x)\boldsymbol{e}_z, \tag{2.5}$$

in which $\boldsymbol{v}$ is the particle velocity vector, $\boldsymbol{u}$ is the fluid velocity vector at the particle location, $C_d = 24(1+0.15Re_P^{0.687})/Re_P$ is the Stokes drag coefficient, $\tau_P = d_P^2\rho_P/18\mu$ is the particle relaxation time (d_P, ρ_P, and μ being particle diameter and density and fluid viscosity respectively), $\boldsymbol{g}$ is gravitational acceleration and $\boldsymbol{e}_z$ is the unit vector in wall-normal direction. All physical quantities have been made dimensionless in terms of wall units based on shear velocity, kinematic viscosity and fluid density. The left-hand side of (2.5) represents particle inertia, and the terms on the right-hand side of (2.5) represent the effects of Stokes drag, gravity and Saffman lift force. The Saffman lift force reproduces the effects of the local gradient of the fluid velocity field $\partial u_x/\partial z$ acting on a rigid spherical particle in a streamwise-oriented, time-dependent shear flow that is a function of the wall-normal direction (Saffman 1965). In (2.5), the lift force term is written according to Saffman (1965) with an additional correction factor $\xi(\epsilon)$ to account for situations where the velocity difference between the particle and the continuous phase becomes larger (McLaughlin 1991). The correction factor

Run	τ_p (ms)	τ_p^+	d_p (μm)	d_p^+
R1	4.35	3.8	40	0.3
R2	32.9	29.1	110	0.825
R3	131.7	116.3	220	1.65

TABLE 1. Parameters relative to the simulation of particle dispersion. The superscript + identifies dimensionless variables.

is computed as follows (McLaughlin 1991):

$$\left.\begin{aligned} \xi(\epsilon) &= \frac{1}{K}[-32\pi^2\epsilon^5 \ln(\epsilon^{-2})],\ \epsilon \leqslant 0.025, \\ \xi(\epsilon) &= \frac{1}{K}[1.418 \arctan(2.8\epsilon^{2.44})],\ 0.025 < \epsilon \leqslant 20, \\ \xi(\epsilon) &= \frac{1}{K}(K - 0.6463\epsilon^{-2}),\ \epsilon > 20, \end{aligned}\right\} \tag{2.6}$$

where $K = 2.225$ and $\epsilon = |\partial u_x^+/\partial z^+|^{0.5} d_P^+ (Re_P)^{-1}$. We have that $\xi(0) = 0$ whereas $\xi(\epsilon)$ becomes equal to unity for high values of ϵ.

Other forces acting on the particle, such as the hydrostatic force, Magnus effect, Basset history force and added mass force are not taken into account since they are assumed to be negligible (orders of magnitude smaller than the three effects considered) because of the specific set of physical parameters of our simulations (Rizk & Elghobashi 1985; Armenio & Fiorotto 2001).

In the present simulations, 48^3 flyash particles, characterized by a particle-to-fluid density ratio equal to 769.23, have been released at randomly chosen locations within the computational box. During the simulation, particles go toward either wall. Comparing the statistics of particle dynamics obtained for the two walls, we found no significant difference, thus indicating that our particle swarm is large enough to ensure meaningful quantitative analysis.

Using samples of 48^3 particles for each diameter, particle Lagrangian velocity statistics (not shown here) become stationary in time after a few particle time constants.

The trajectories of the particles were tracked individually through integration of (2.5) by an explicit method, using the channel flow DNS code to supply the fluid velocity field at each time step. The initial velocities of the particles were set equal to the interpolated fluid velocities at each particle location.

In table 1, dimensionless and dimensional parameters characterizing the tracked particles are reported. The three particle sets considered here are large compared to those examined by other authors, who considered particles in the range $\tau_P^+ = 0 - 3$ (McLaughlin 1989; Brooke *et al.* 1992; Pan & Banerjee 1996; Uijttewaal & Oliemans 1996). Particle behaviour changes dramatically over this range of particle relaxation times. In particular, particles with τ_P^+ close enough to zero will behave like fluid parcels, showing no preferential concentration. This is required to agree with mass conservation for the continuous phase (Brooke *et al.* 1992; Uijttewaal & Oliemans 1996).

Particles with finite inertia will respond to the coherent vortical structures of the boundary layer in different ways. Following Pan & Banerjee (1996), the particle samples which seem to respond 'best' to the specific size of the structures are characterized by a dimensionless relaxation time around $\tau_P^+ = 1.0$.

Notice that (2.5) does not include wall effects: when the distance of the particle from the closest wall becomes small compared to particle size, the actual mechanism of deposition is complicated by the possible effect of different surface-related phenomena (McLaughlin 1991). In our calculations, these phenomena were not taken into account and we simply considered that a particle is elastically reflected away from the wall when its centre is less than a distance $d_P/2$ from the boundary. Perfect elastic reflection, i.e. where no dissipation occurs during the collision, is at the other extreme with respect to the perfectly absorbing wall model, in which particle kinetic energy is completely lost during the collision. Real cases usually fall between these limiting situations. Since one of the objects of our work is to understand the reasons for particle trapping in the wall layer, the fully elastic rebound is the most conservative assumption.

3. Results and discussion

3.1. *Particle distribution in the boundary layer*

We investigated turbulent transfer mechanisms and segregation of inertial particles in a boundary layer over a flat vertical wall. The response of rigid, pointwise particles to turbulence is related to the Stokes number, defined as the ratio between the particle relaxation time τ_P and some representative time scale of the turbulent fluid motion τ_f (Crowe, Gore & Troutt 1988): thus, the controlling variable was τ_P (or diameter d_P, since all the other parameters were kept constant during the simulations).

In figure 1(*a–d*), the instantaneous top view of particle distribution for $\tau_P^+ = 3.8$ particles is shown at different times of the simulation. For clarity of presentation, we show only 1 in 2 particles. At time $t^+ = 0$ (figure 1*a*), particles are uniformly distributed in the entire computational domain. After 706 dimensionless wall time units (figure 1*b*), most of the particles have been swept towards the wall. Particles which remain in the centre of the channel are promptly segregated into large elongated structures from which they are efficiently transferred toward the wall region. These structures are usually located in the channel core and appear to be surrounded by roughly circular regions in which hardly any particles are present. In figure 1(*c*, *d*), taken at 1412 and 2118 dimensionless wall time units, the non-random fashion of particle clustering is more evident.

Notice that particle clusters are seen to approach the walls through preferential avenues and to strike the wall at an angle of approximately 45°, as indicated by the black arrows. Since, in the present upflow configuration, gravity does not affect particle deposition significantly, this behaviour is probably due to turbulence structures and has also been observed in pipe flow boundary layers (Cerbelli *et al.* 2001). The same qualitative behaviour is observed for both $\tau_P^+ = 29.1$ and $\tau_P^+ = 116.3$ particles (not shown here).

In figure 2(*a–d*), the time evolution of mean particle concentration for all particle sizes is shown as a function of the distance z^+ from the channel wall. A logarithmic scale is used to expand the near-wall region and to capture the different behaviour of particle transfer. Consider that, in dimensionless wall units (see table 1), particles of the three dimensions investigated touch the wall at $z^+ = 0.15$, $z^+ = 0.4125$ and $z^+ = 0.825$ respectively (the last point of the plot). Starting from the initial uniform distribution, concentration profiles were computed at fixed time intervals by subdividing the channel into 65 slabs (through Chebyshev polynomials) and counting the fraction of particles that fell within each slab, i.e. by averaging over the streamwise and

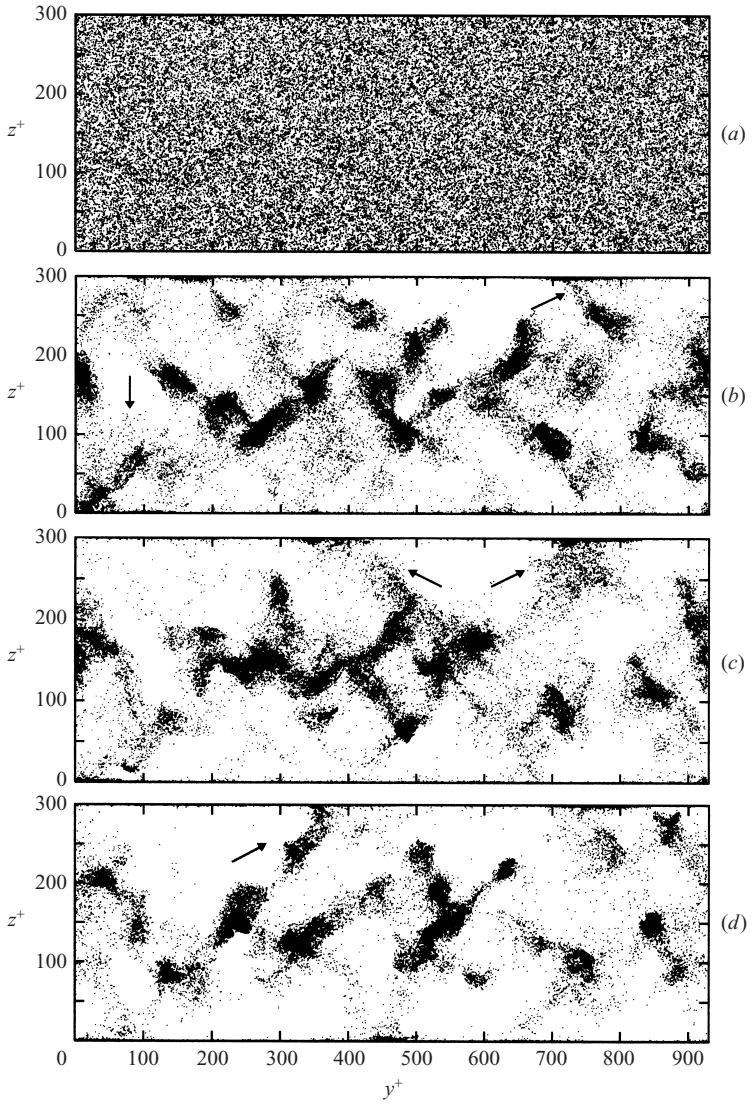

FIGURE 1. Top view of instantaneous distribution for $\tau_p^+ = 3.8$ particles at different times: (*a*) $t^+ = 0$, (*b*) $t^+ = 706$, (*c*) $t^+ = 1412$, (*d*) $t^+ = 2118$. Notice that particles in the centre of the channel are promptly segregated into large elongated structures surrounded by roughly circular regions in which hardly any particles are present.

spanwise coordinates, x and y, respectively. For each particle size, there is an expected accumulation in the near-wall region, which increases in time. This wall segregation occurs quickly even though it is slower for larger particles (after 2118 time steps, which correspond to about 2.4 s, 42% of $\tau_P^+ = 3.8$ particles enter the viscous sublayer; the percentage is almost the same – about 41% – for $\tau_P^+ = 29.1$ particles and decreases to 29% for $\tau_P^+ = 116.3$ particles).

As already observed in pipe flow geometry (Cerbelli *et al.* 2001), particles seem to accumulate in a region very close to the wall, where the particle number density profile develops a maximum, which shifts toward the wall over time. This behaviour can be viewed as the consequence of non-uniform turbulence advection mechanisms,

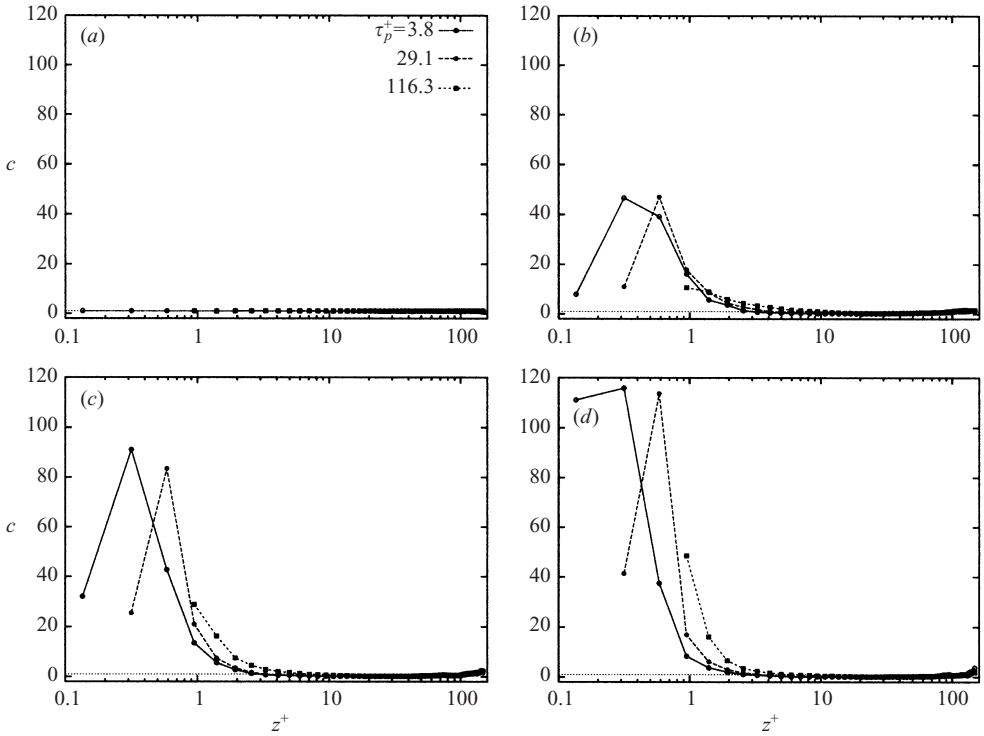

FIGURE 2. Number density distribution for $\tau_p^+ = 3.8$, $\tau_p^+ = 29.1$ and $\tau_p^+ = 116.3$ particles at different times: (*a*) $t^+ = 0$, (*b*) $t^+ = 706$, (*c*) $t^+ = 1412$, (*d*) $t^+ = 2118$.

whose intensity decreases to very low values in the near-wall region. In other words, from a macroscopic, engineering viewpoint, particle transport toward the wall can be roughly envisioned as a two-stage process characterized by different time scales. Particles are driven away from the outer flow region by energetic turbulent convective mechanisms, accumulate close to the wall, and are then slowly transported toward the wall.

As demonstrated in previous works (Young & Leeming 1997; Zhang & Ahmadi 2000), the Saffman lift force acts as to favour heavy particle deposition if particles move faster than the fluid – downward flow – whereas it slows wall segregation of heavy particles when particles move slower than the fluid – upward flow, as in the present case. The effects of the Saffman lift force becomes weaker as particle inertia increases (Wang & Squires 1996; Uijttewaal & Oliemans 1996). We made simulations without Saffman lift force for the three sets of particles considered and we found that particle fluxes to the wall decrease a little, this effect being smaller for larger particles. Concentration profiles for no-lift simulations (not shown here) were qualitatively similar, and little different quantitatively, from those in figure 2.

Particle migration to the wall in turbulent boundary layers has been observed previously (Caporaloni *et al.* 1975; Reeks 1983) and the name turbophoretic drift was given to this phenomenon, which is extremely relevant for a number of industrial and environmental applications. The mechanisms leading to these strong particle net fluxes to the wall are precisely the aim of this work and we will try to investigate this issue by examining particle dynamics in connection with the dynamics of wall coherent structures.

3.2. *Particle distribution in the wall region*

Even when segregated in the wall region, particles do not attain a uniform distribution in the spanwise wall-parallel direction. As reported previously (Pedinotti *et al.* 1992; Eaton & Fessler 1994; Pan & Banerjee 1996; Zhang & Ahmadi 2000) particle positions tend to correlate with the instantaneous location of the lower values of the streamwise velocity – low-speed streaks. This behaviour is confirmed in figure 3, in which the instantaneous distribution of particles in the region between the wall and $z^+ = 4$ is shown superimposed onto the contours of the streamwise fluctuation velocity u', on a (x, y)-plane close to the wall ($z^+ = 4$). Figure 3(a–c) corresponds to the particle concentration profiles shown in figure 2, calculated at time $t^+ = 2118$ from the beginning of the simulation. We tried to reproduce the particles with their diameters in the correct reciprocal dimensional scale. Even though we could not scale particle diameter to the box dimensions – the smallest particles would have been invisible – this should give a physical rendering of the phenomenon. As reported in previous works (Pedinotti *et al.* 1992; Kaftori *et al.* 1995*a*, *b*; Pan & Banerjee 1996; van Haarlem *et al.* 1998), we can observe that particles tend to line up along the low-speed streaks – in blue – and tend to avoid the high-speed regions – in red. Comparing our results to those by Pedinotti *et al.* (1992) or by Zhang & Ahmadi (2000), we may observe that particle lines tend to be straighter and less meandering. The first reason is that particle inertia is larger in our simulations. Second, as observed by Zhang & Ahmadi (2000), gravity induces a bias in the streamwise direction (Tchen 1947; Wells & Stock 1983). As expected, this effect is more pronounced for larger particles.

To give a quantitative measure of particle preferential distribution in the low-speed streaks, in figure 4 we show the particle number density distribution as a function of the fluctuating streamwise velocity, u', in the wall region ($z^+ \leqslant 10$). We computed the particle number density distribution as a function of the fluctuating streamwise velocity as follows: (i) we subdivided the region $z^+ \leqslant 10$ into 10 equally spaced slabs and calculated the average streamwise velocity of the fluid $\bar{u}_{slab}(z)$ in each slab, (ii) we determined the slab containing the particle, (iii) we computed the local streamwise velocity fluctuation of the fluid $u'(x, y, z) = u(x, y, z) - \bar{u}_{slab}(z)$ at the position of the particle, (iv) we counted the number of particles associated with each value of $u'(x, y, z)$ and normalized it by the total number of particles located in each slab.

From figure 4, it appears that particles tend to attain a preferential distribution in the regions of lower-than-mean fluid velocity. There is also evidence of an effect of particle relaxation time: the position of larger particles seems to correlate better with regions of lower negative u'. The tendency of inertial particles to accumulate in the low-speed regions may support a possible use of particles as smart roughness (Pan & Banerjee 1996). In real situations, characterized by a two-way coupling between particles and fluid, the presence of particles would increase the inertia of the low-speed streaks. Since low-speed streak stability to lateral perturbation has an impact on the wall turbulence regeneration cycle (Schoppa & Hussain 1996, 1997, 2000; Soldati & Marchioli 2001; Soldati 2002), the presence of particles of specific inertia or size in turbulent boundary layers might be exploited to tune wall transfer mechanisms.

3.3. *Particle transfer fluxes*

As observed already (see figure 2), particle transfer to the wall is a remarkably efficient phenomenon. In figure 1, we observed preferential pathways of particles striking the wall at 45°. These pathways correspond to coherent advective motions which

scale with the buffer layer and are the instantaneous realizations of the Reynolds stresses. The relationships between these advective motions and particle transfer to the wall may be elucidated through quadrant analysis (Wallace, Eckelmann & Brodkey 1972). In the (u', w') plane, with positive w' directed outward, the Reynolds stress is produced by four types of events: first quadrant events (I), characterized by outward motion of high-speed fluid, with $u' > 0$ and $w' > 0$; second quadrant events (II), characterized by outward motion of low-speed fluid, with $u' < 0$ and $w' > 0$, which are usually called *ejections*; third quadrant events (I), characterized by inward motion of low-speed fluid, with $u' < 0$ and $w' < 0$; and finally, fourth quadrant events (IV), which represent motions of high-speed fluid toward the wall, with $u' > 0$ and $w' < 0$, and are usually called *sweeps*. Ejections and sweeps contribute to negative Reynolds stress, i.e. to increase turbulence production, whereas first and third quadrant events contribute to positive Reynolds stress, i.e. to decrease turbulence production. The presence of a sweep corresponds to a local increase of the shear stress at the wall whereas the presence of an ejection corresponds to a local decrease of the shear stress at the wall.

Here, we have two aims: the first is to verify whether sweeps and ejections are the mechanisms by which particles are transferred toward the wall and are entrained into the outer flow. The second is to quantify the role of sweeps and ejections in determining particle fluxes to and from the wall layer.

In figure 5, we highlight the spatial correlation of the location of sweeps and ejections and the preferential locations where particles penetrate and exit the wall layer. In figure 5(*a*), we show the probability density functions of $u'w'$ events plotted as a function of the local wall shear stress, which is normalized to its average value. As can be observed from figure 5(*a*), sweeps and ejections are separated by a crossover level of the wall shear stress, the sweeps corresponding to high-shear-stress regions and the ejections corresponding to low-shear-stress regions. A slight overlapping between the two distributions exists and the value 1.0 of the normalized shear stress separates 'high-' and 'low-' shear-stress regions. A similar trend is obtained for the distributions of first and third quadrant events, which, however, are much smaller in area. In figure 5(*b–d*), we show the probability density function of particles having positive wall-normal velocity – toward the wall – and negative wall-normal velocity – toward the outer flow – plotted as a function of the local wall shear stress.

As observed in figure 2, the particle distribution along the wall-normal coordinate changes with time, and particle fluxes toward the wall and away from the wall therefore change with time. We tried to quantify the fluxes toward and away from the wall by counting the instantaneous number of particles that cross a specific monitor slab calculated at two different simulation times, $t_1^+ = 1342$ and $t_2^+ = 2048$. We counted the particles having positive or negative wall-normal velocity instantaneously present in the monitor slab of 10 wall units (from $z^+ = 5$ to $z^+ = 15$ from the wall). The profiles reported in figure 5(*b–d*) were computed from

$$N_{in/out} = \frac{\sum_{i=1}^{20} n_i}{TA}, \tag{3.1}$$

where n_i is the number of particles with negative/positive wall-normal velocity w_P counted at the measuring points per unit time, T is the length of the time averaging period and A is the measuring area (Kaftori *et al.* 1995*b*).

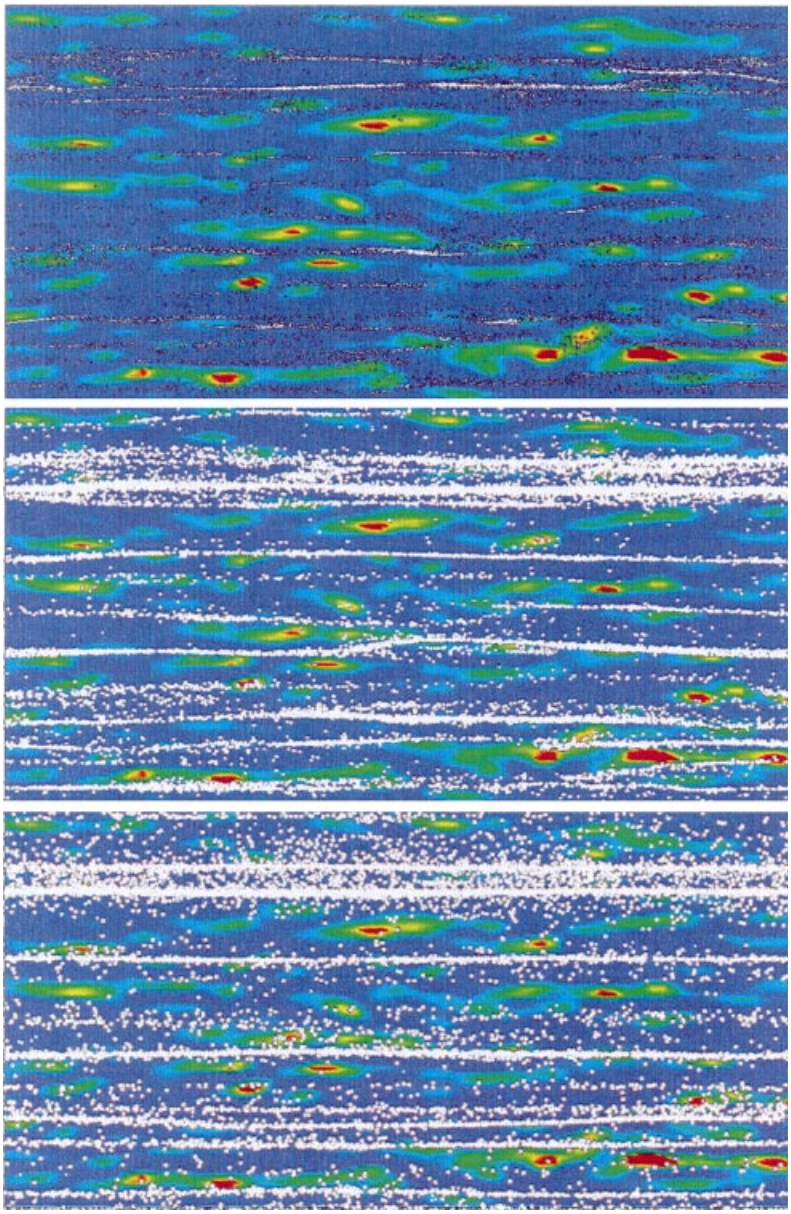

FIGURE 3. Distribution of particles in the wall region. Coloured contours of streamwise fluctuating velocity u' (red indicates high positive values for u', blue indicates high negative values for u') on a horizontal plane at $z^+ = 4$ from the wall, show the streaky structures. Particles comprised between $z^+ = 4$ and the wall are shown. (*a*) $\tau_p^+ = 3.8$ particles, (*b*) $\tau_p^+ = 29.1$ particles, (*c*) $\tau_p^+ = 116.3$ particles.

To have a larger particle set for calculating particle fluxes, we averaged fluxes over a short time of length $\Delta t^+ = 142$ (20 instantaneous realizations of the flow field), centred around t_1^+ and t_2^+. For brevity, we will refer to the instantaneous number of particles that cross a specific monitor slab as particle flux (Kaftori *et al.* 1995*b*).

All plots are normalized by the peak value obtained for the $\tau_P^+ = 3.8$ particles flux toward the wall, which appears to be the most intense. For $\tau_P^+ = 3.8$ and $\tau_P^+ = 29.1$

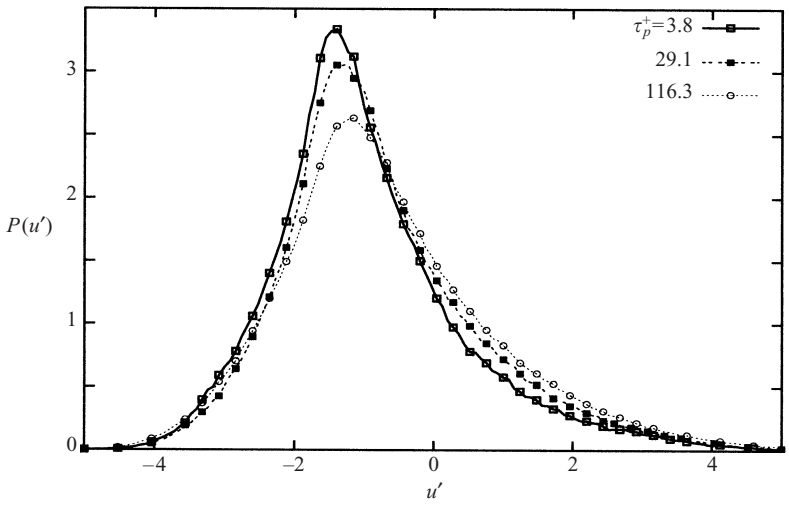

FIGURE 4. Particle number density distribution as a function of fluctuating streamwise velocity, u', in the wall region ($z^+ \leqslant 10$) for $\tau_p^+ = 3.8$, $\tau_p^+ = 29.1$ and $\tau_p^+ = 116.3$ particles. The particle number density distribution peaks for negative values of fluctuating streamwise velocity showing that near the wall particles are found preferentially in low-streamwise-velocity regions.

particles, fluxes to the wall and away from the wall are similar, thus confirming the similar behaviour with time of particle distribution shown in figure 2. Particle fluxes toward the wall decrease a little with time for the smaller particles, but increase for the larger particles. As shown in figure 2, larger particles take a longer time to change their distribution. Particle flux away from the wall decreases with time for smaller particles and remains roughly constant for the larger particles.

Two main conclusions can be drawn from figure 5(*b–d*). First, it is confirmed that, regardless of particle size, a strong correlation exists between particle fluxes to the wall (N_{in}) and high-wall-shear-stress regions, which correspond to sweep events; low-wall-shear-stress regions correspond to ejection events and are well correlated with off-the-wall particle fluxes (N_{out}). Second, fluxes to the wall always have a greater intensity than fluxes toward the outer flow, this trend being enhanced when particle size is smaller. This suggests that, particularly in the case of smaller particles, ejections are somehow unable to lift up all the particles that sweeps drive toward the wall, i.e. particles tend to settle in a sediment layer at the wall, which roughly corresponds to the viscous sublayer. This by no means implies that larger inertia particles are more efficiently transferred far from the wall by ejections. It merely indicates that such particles may find other ways to exit the wall layer. This is apparent on considering a perfectly elastic particle–wall interaction: larger particles gain greater momentum in the sweeps and do not always need organized structures to be driven out from the wall region. They may simply bounce off the wall. To support this observation, we computed the normalized particle flux profiles ($N_{out\ abs}$) in the case of perfectly absorbing wall (i.e. particles do not bounce off the wall) at time t_2^+. The overall intensity of upward particle flux – i.e. the area under the curve – for $\tau_P^+ = 116.3$ particles undergoes a 17.4% decrease compared with the case of perfectly reflecting wall. This decrease is smaller for smaller particles (9.8% for $\tau_P^+ = 29.1$ particles and 7.2% for $\tau_P^+ = 3.8$ particles).

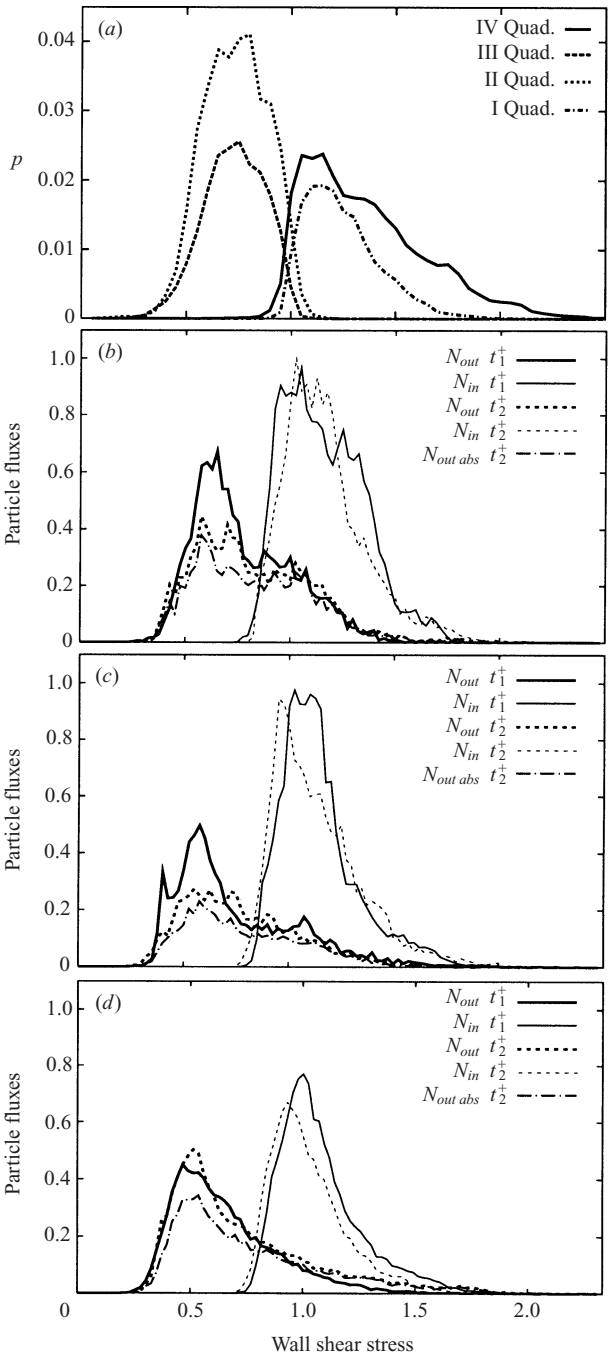

FIGURE 5. Correlation between particle fluxes in and out of the wall layer and wall shear stress distribution. (*a*) Probability distribution of $u'w'$ events in I, II, III and IV quadrant events versus wall shear stress. (*b*), (*c*) and (*d*) Correlation of the normalized particle fluxes in and out of the wall layer with wall shear stress for $\tau_p^+ = 3.8$, $\tau_p^+ = 29.1$ and $\tau_p^+ = 116.3$ particles, respectively.

3.4. *Instantaneous particle transfer mechanisms*

As discussed, particle fluxes are dominated by the same coherent flow structures that control momentum transfer to the wall. The shear stress at the wall is governed by the strongly coherent flow structures generated by the quasi-streamwise vortices, i.e. sweeps and ejections. From the previous results, it appears that particles are driven to the wall by the sweeps and are entrained away from the wall by the ejections. However, since the particle distribution in the wall-normal direction changes over time, increasing in the wall layer and decreasing in the outer layer, fewer particles will be available to be transferred to the wall, the reverse being true for particle transfer away from the wall. The efficiency of a coherent convective motion is thus conditioned by the presence of particles. Here, we will try to establish the efficiency of particle transfer mechanisms to the wall and away from the wall.

By analogy with momentum transfer (Orlandi & Jimenez 1994), mass transfer (De Angelis *et al.* 1997) and heat transfer (Lu & Hetsroni 1995), we focused on the effects of strongly coherent sweep and ejection events on particle transfer and considered the wall layer up to $z^+ = 12$ (Lombardi, De Angelis & Banerjee 1996). Within this layer, we chose five monitor (x, y)-planes (the heights away from the wall of these planes are $z^+ = 4$, $z^+ = 6$, $z^+ = 8$, $z^+ = 10$, $z^+ = 12$). At each time step considered, we recorded the velocity components on the five monitor planes at each collocation point. To count only those events with substantial spatial coherence, an event is recorded, at some point $(\bar{x}, \bar{y})$, when on at least four of the five monitor planes, $u'w'$ belongs to the same quadrant (Lombardi *et al.* 1996). Considering only sweeps and ejections which contribute to the negative turbulence-producing part of the Reynolds stress, sweeps contribute to a larger fraction of the negative Reynolds stress for $z^+ < 11$ whereas ejections contribute to a larger fraction of the negative Reynolds stress for $z^+ > 11$ (Willmarth & Lu 1972; Wallace *et al.* 1972; Kim *et al.* 1987). We therefore focused on the crossover plane between sweep/ejection dominance, at $z^+ = 11$, and we characterized all particles in the region between $z^+ = 10$ and 12 from the wall by their velocity w_P, which is negative toward the wall and positive toward the outer flow.

In figure 6(*a*), we show the instantaneous position of strongly coherent sweeps, characterized by the isocontours corresponding to $u'w' < 0$ in dimensionless units, and the instantaneous position of all the $\tau_P^+ = 3.8$ particles directed toward the wall. There is evidence of a strong correlation between particles with negative w_P and sweeps, since only a small fraction of the particles falls out of sweep regions. In figure 6(*b*), the position of the particles with positive w_P is shown together with the instantaneous position of strongly coherent ejections, characterized again by the isocontours of negative $u'w'$. There is evidence of a strong correlation between the position of an ejection and the location from which particles exit the wall layer. The same type of visualizations for the larger particle sets (not shown here) confirm the qualitative results of figure 6.

Our aim now is to quantify the visual observations of figure 6 and, in particular, to determine the fraction of particle fluxes toward the wall and away from the wall actually driven by the sweeps and the ejections, respectively. Thus, we computed, at fixed time intervals, the correlation between the wall-normal velocity of particles located in the wall layer up to $z^+ = 12$ and the quadrant events occurring at each particle position. We evaluated the average area on the monitor plane and, sampling 50 instantaneous realizations, we found that about 60% of the monitor plane is occupied by the strongly coherent sweeps and ejections.

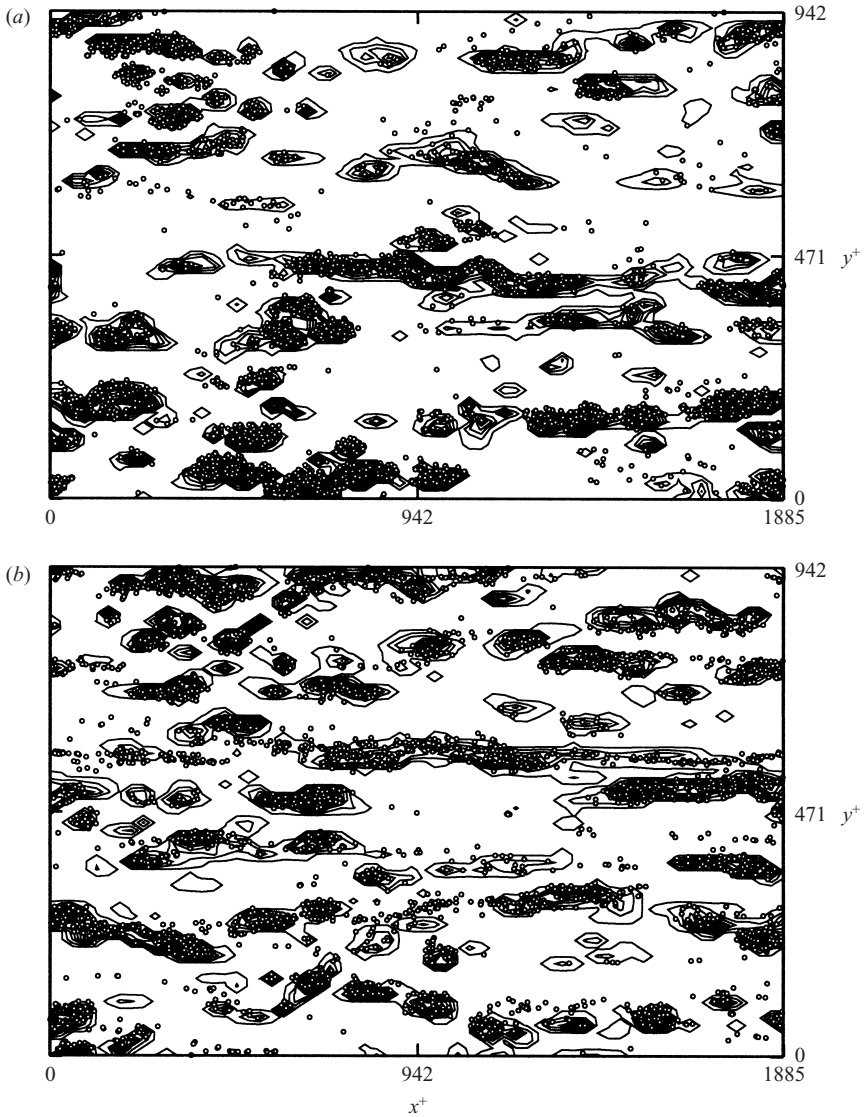

FIGURE 6. Instantaneous correlation between strongly coherent sweeps and ejections and $\tau_p^+ = 3.8$ particle fluxes toward the wall and away from the wall: (*a*) instantaneous correlation between strongly coherent sweep events and particle fluxes toward the wall at $z^+ = 11$, (*b*) instantaneous correlation between strongly coherent ejection events and particle fluxes away from the wall at $z^+ = 11$.

However, if we count the number of particles that cross the monitor plane and observe where they cross it, we find that, for $\tau_P^+ = 3.8$ particles, of the overall number of 42 280 particles crossing the plane in both directions, 98.05% of the particles are located in regions where we find either a strongly coherent sweep or a strongly coherent ejection. For the $\tau_P^+ = 29.1$ particles, this percentage is 98.01% of the overall number of 41 090 particles transferred, whereas for the $\tau_P^+ = 116.3$ particles, the percentage is 91.51% of the overall number of 28 961 particles transferred. Even for the largest particles, it is apparent that the strongly coherent events control particle fluxes to the wall and away from the wall, and represent almost exclusively inlet and outlet channels to and away from the wall region.

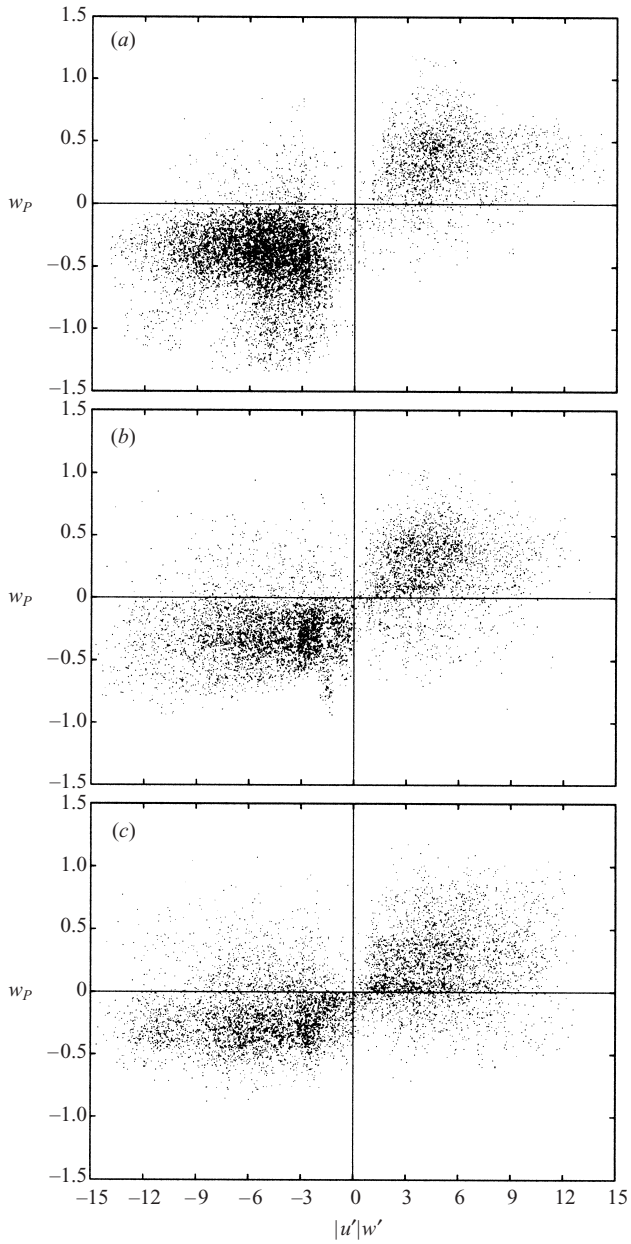

FIGURE 7. Time-averaged correlation between strongly coherent events and particle fluxes toward the wall and away from the wall for (*a*) $\tau_p^+ = 3.8$ particles, (*b*) $\tau_p^+ = 29.1$ particles, (*c*) $\tau_p^+ = 116.3$ particles.

We quantified the efficiency of the transfer mechanisms as shown in figure 7, where negative values of $|u'|w'$ are associated with strongly coherent sweeps and positive values of $|u'|w'$ are associated with strongly coherent ejections. To include only events with statistically significant occurrence, calculations were made over 250 instantaneous flow realizations (covering an overall time from $t^+ = 353$ to $t^+ = 2118$). For clarity of presentation, we chose to show only 1 in 5 points to represent the quadrant point distribution in figure 7.

w_P	$\lvert u'\rvert w'$	Event type	$\tau_p^+(\%) = 3.8$	$\tau_p^+(\%) = 29.1$	$\tau_p^+(\%) = 116.3$
$P_S^d < 0$	< 0	Sweep	96.74%	92.26%	81.22%
$P_E^d < 0$	> 0	Ejection	3.26%	7.74%	18.78%
$P_E^u > 0$	> 0	Ejection	90.24%	84.14%	65.82%
$P_S^u > 0$	< 0	Sweep	9.76%	15.86%	34.18%
$P_N^d < 0$	—	None	1.54%	1.56%	7.8%
$P_N^u > 0$	—	None	3.23%	3.36%	9.52%

TABLE 2. Probabilities representing the correlation between particle wall-normal velocity w_P and sweep events ($|u'|w' < 0$) or ejection events ($|u'|w' > 0$) at plane $z^+ = 11$. Probabilities are defined as follows: $P_S^d = P(|u'|w' < 0 \mid w_P < 0)$, $P_E^d = P(|u'|w' > 0 \mid w_P < 0)$, $P_E^u = P(|u'|w' > 0 \mid w_P > 0)$, $P_S^u = P(|u'|w' < 0 \mid w_P > 0)$. The fraction of particles with negative or positive wall-normal velocity which are located in non-sweep/non-ejection environments is represented by P_N^d and P_N^u respectively.

For $\tau_P^+ = 3.8$ particles (figure 7*a*), we find that 30 456 out of 31 482 particles with negative wall-normal velocity w_P are located within $|u'|w' < 0$ regions whereas only 1026 are located in $|u'|w' > 0$ regions. This indicates that almost all the particles with a downward trajectory are engulfed in a sweep (the probability for a particle to be entrained in a sweep conditioned by having wall-directed velocity is $P_S^d = P(|u'|w' < 0 \mid w_P < 0) = 96.74\%$) and only a small proportion is involved in an ejection ($P_E^d = P(|u'|w' > 0 \mid w_P < 0) = 3.26\%$). Considering the semi-plane $w_P > 0$, 8820 out of 9974 particles are located in $|u'|w' > 0$ regions whereas 954 are located in $|u'|w' < 0$ regions. This indicates that the percentage of ejection-entrained particles with a trajectory away from the wall is equal to $P_E^u = P(|u'|w' > 0 \mid w_P > 0) = 90.24\%$ whereas the percentage of such particles which are entrained in a sweep is equal to $P_4 = P(|u'|w' < 0 \mid w_P > 0) = 9.76\%$.

For the $\tau_P^+ = 29.1$ particle case (see figure 7*b*), the plotted points are subdivided as follows: 30 769 particles characterized by $w_P < 0$ (28 388 located in $|u'|w' < 0$ regions, corresponding to $P_S^d = 92.26\%$, and 2381 located in $|u'|w' > 0$ regions, corresponding to $P_E^d = 7.74\%$) and 9503 particles characterized by $w_P > 0$ (7996 located in $|u'|w' > 0$ regions, corresponding to $P_E^u = 84.14\%$ and 1507 with $w_P < 0$, corresponding to $P_4 = 15.86\%$).

In figure 7(*c*), the correlation between particle wall-normal velocity and sweep/ejection events is shown for $\tau_P^+ = 116.3$ particles: 15 966 particles have $w_P < 0$ (12 972 located in $|u'|w' < 0$ regions, corresponding to $P_S^d = 81.22\%$, and 2994 located in $|u'|w' > 0$ regions, corresponding to $P_E^d = 18.78\%$) and 10 536 have $w_P > 0$ (6936 located in $|u'|w' > 0$ regions, corresponding to $P_E^u = 65.82\%$ and 3600 located in $|u'|w' < 0$ regions, corresponding to $P_S^u = 34.18\%$).

These results are summarized in table 2. It is interesting to observe that the overall particle number driven toward the wall is similar for the smaller particle size (31 482 and 30 769 for the $\tau_P^+ = 3.8$ and $\tau_P^+ = 29.1$ particles respectively), whereas it decreases abruptly for the largest particles (15 966 for the $\tau_P^+ = 116.3$ particles). This may be due to the influence of the stronger structures in the region beyond $z^+ = 11$. These structures impart considerable momentum to particles and may contribute to decorrelate larger particles from the sweeps. Particles behave as a low-pass filter and respond to perturbations of the appropriate time scale. The larger the particle, the larger the structure has to be to modify the particle trajectory. Rather surprisingly, we observe that the overall particle number driven away from the wall layer is almost

independent of particle size (9974, 9503 and 10536 for the $\tau_P^+ = 3.8$, $\tau_P^+ = 29.1$ and $\tau_P^+ = 116.3$ particles respectively).

From the data in table 2, we also notice that smaller particles follow closely sweeps and ejections and their transfer rates are well-correlated with the instantaneous realizations of turbulent Reynolds stresses. The larger the particle size, the weaker the correlation and a larger fraction of particles is found to travel to the wall in an ejection or to travel away from the wall in a sweep. It is particularly relevant to observe that a large fraction – 34.18% – of the larger particle set travels toward the outer flow in sweep environments. As observed before, larger particles may return toward the outer flow simply by bouncing elastically on the wall by exploiting the large momentum gained.

Results similar to those presented here on particle fluxes were previously obtained by Kaftori *et al.* (1995*b*), who ascribed particle behaviour to the gravitational pull experienced by the particles in a horizontal turbulent boundary layer. In our simulations, the force due to gravity cannot directly cause particle deposition at the wall and the buildup of particles in a sediment layer must be explained, from a physical viewpoint, by different mechanisms, in which near-wall turbulent coherent structures play a crucial role.

3.5. *Turbulent structures and particle trapping mechanism*

In the previous sections, we presented both qualitative and quantitative results to put in evidence the mechanisms by which particles are transferred to the wall by the sweeps and are eventually re-entrained into the outer flow by the ejections. We also determined how the strongly coherent $u'w'$ events influence particle fluxes. The picture is that particles enter the wall layer advected by the strongly coherent sweeps and exit the wall layer advected by the strongly coherent ejections. However, exit fluxes are much weaker than incoming fluxes. We will try to address that issue in this section.

Specifically, our aim is to explain, from a physical viewpoint, the mechanisms for particle segregation within the boundary layer. To this end, we have to link all the phenomena observed to the dynamics of the near-wall turbulent vortical structures.

The vortical structures which dominate the wall layer dynamics are the aforementioned quasi-streamwise vortices, which generate sweeps on the downwash side, and ejections on the upwash side. In turn, ejections contribute to the maintenance of the lifted low-speed streaks on the upwash side of the quasi-streamwise vortices. Recent results (Schoppa & Hussain 1996, 1997; Soldati & Marchioli 2001) show that clockwise and counterclockwise, quasi-streamwise vortices flank the low-speed streak as a staggered array in most cases. Only rarely do a clockwise and a counterclockwise quasi-streamwise vortex appear together. This scenario is consistent with the mechanism proposed by Adrian *et al.* (2000) who identify and characterize the fundamental role of packets of hairpin vortices travelling at the same convection velocity in the turbulence regeneration mechanism. We remark here that gravity does not play a direct role in trapping particles at the wall and yet a large number of particles accumulate in the region below $z^+ = 5$ (see also figure 2).

Considering the state of the art on turbulence structures at the wall and the results we obtained in the previous section we observe that: (i) among all the second and fourth quadrant events, the strongly coherent sweeps and ejections are responsible for transferring towards and away from the wall most of the particles of the size range we investigated; (ii) the strongly coherent sweeps and ejections are generated by the strongly coherent near-wall quasi-streamwise vortices; (iii) in low-Reynolds-

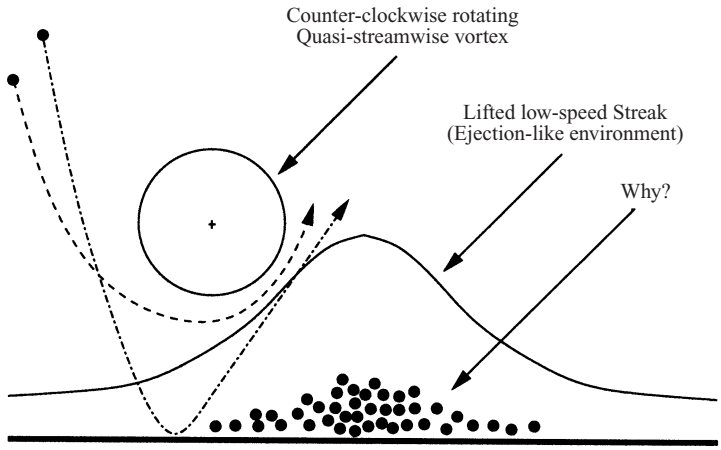

FIGURE 8. Schematic of one possibly unsatisfactory mechanism for particle transfer to the wall and away from the wall. Following this mechanism, a large-scale coherent quasi-streamwise structure can generate a strongly coherent sweep to bring particles to the wall and a strongly coherent ejection to drive particles to the outer flow. This mechanism does not explain the accumulation of particles at the wall under the low speed streaks.

number turbulent boundary layers, the strongly coherent archetype quasi-streamwise vortices have been identified and sized by several authors (Guezennec *et al.* 1989; Lyons *et al.* 1991; Brooke & Hanratty 1993; Schoppa & Hussain 1996, 1997; Jeong *et al.* 1997; Jimenez & Pinelli 1999; Soldati & Marchioli 2001). In most cases, these vortices are not paired with an equal-size parallel counter-rotating vortex. Thus, we can use the schematic in figure 8 to pose a fundamental question. With reference to figure 8, we can envision the following cycle for particles initially in the outer flow: if a particle is captured by a sweep, it moves along a curved trajectory around the quasi-streamwise vortex generating the sweep, approaches the wall and moves between the vortex and the wall. During this phase, the particle may touch the wall or not. Then, the particle is on the upwash side of the vortex and is subject to the influence of the ejection. The next step involves passing through the lifted low-speed streak and exiting from the wall layer. Considering in particular the conservative conditions of our simulations, with perfectly elastic rebound, particles should migrate toward the surface of the lifted low-speed streak, which is an ejection-like environment, and find an ejection strong enough to drive them into the outer flow. Yet most of the particles remain trapped under the lifted low-speed streak.

To investigate the mechanisms leading to particle accumulation under the lifted low-speed streaks, we examined a large number of snapshots showing the action of quasi-streamwise vortices on particle transfer in the wall region. We show one of these in figure 9(*a*), which focuses on a y, z window of the computational domain extracted for the length of one streamwise cell (dimensions are $30 \times 58 \times 108$ in dimensionless wall units) at time $t^+ = 1412$. The main item in this picture is the green counterclockwise-rotating quasi-streamwise vortex characterized by positive ω_x vorticity, centred at $z^+ = 36$. We also show, for the $\tau_P^+ = 3.8$ case, the particles with negative w_P – directed to the wall – with black circles, the particles with positive w_P – directed away from the wall – with blue circles and the particles with w_P almost zero – $|w_P| < 10^{-3}$ in wall units – with open circles. The action of the large vortex in transferring the black particles to the wall and the blue particles away from the wall is apparent. Particles with negligible wall-normal velocity accumulate under

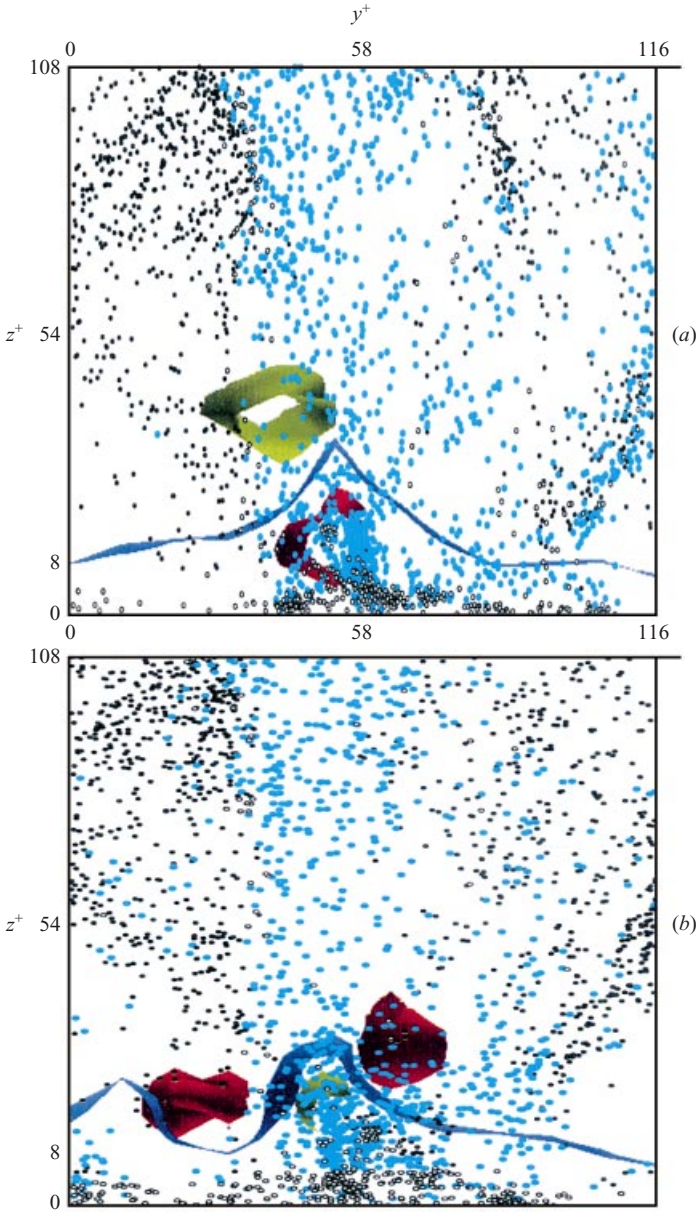

FIGURE 9. Snapshots of particle distribution and turbulent coherent structures in the near-wall region at (*a*) $t^+ = 1412$ and (*b*) $t^+ = 1450$ respectively. Green isosurfaces indicate counterclockwise-rotating vortices, red isosurfaces indicate clockwise-rotating vortices, blue isosurfaces indicate low-speed streaks. Most of the ascending particles (black dots) are located in the region between a mature vortex and a newly born vortex. Most of the descending particles (blue dots) are concentrated on one side of the mature vortex. Particles trapped in the wall layer (particles with $|w_P| < 10^{-3}$) are shown with open circles.

the lifted low-speed streak, which we show with a blue isosurface indicating a streamwise velocity value of $0.56U_C$ (Kim *et al.* 1987), where $U_C = 16.76$ is the centreline velocity. The low-speed streak appears to be lifted by the counterclockwise quasi-streamwise vortex.

The counterclockwise quasi-streamwise vortex is visualized by the streamline rotation vector $\boldsymbol{\Omega}$, which is based on the identification of flow regions where the rate-of-deformation tensor $\partial u_i/\partial x_j$ exhibits complex eigenvalues (Perry & Chong 1987; Chong, Perry & Cantwell 1990; Jeong & Hussain 1995). The vector $\boldsymbol{\Omega}$ is defined as follows:

$$\boldsymbol{\Omega} = \mathrm{Im}(\lambda_c)\frac{\boldsymbol{e}_{\lambda_r}}{|\boldsymbol{e}_{\lambda_r}|}\frac{\boldsymbol{e}_{\lambda_r}\cdot[\mathrm{Re}(\boldsymbol{e}_{\lambda_c})\times\mathrm{Im}(\boldsymbol{e}_{\lambda_c})]}{|\boldsymbol{e}_{\lambda_r}\cdot[\mathrm{Re}(\boldsymbol{e}_{\lambda_c})\times\mathrm{Im}(\boldsymbol{e}_{\lambda_c})]|}, \tag{3.2}$$

where $\mathrm{Im}(\lambda_c)$ is the imaginary part of the pair of complex eigenvalues, $\mathrm{Re}(\boldsymbol{e}_{\lambda_c})$ and $\mathrm{Im}(\boldsymbol{e}_{\lambda_c})$ are the real part and the imaginary part of the conjugate complex eigenvectors corresponding to the complex eigenvalues, $\boldsymbol{e}_{\lambda_r}$ is the eigenvector corresponding to the real eigenvalue λ_r. The vector $\boldsymbol{\Omega}$ is related to the streamline rotation and represents the strength and direction of the rotation of the streamlines. We drew an isosurface plot of $\boldsymbol{\Omega}$ selecting a value equal to 25% of the instantaneous maximum of $\boldsymbol{\Omega}$, which is high enough to capture only the strong vortices (Lombardi *et al.* 1996; Soldati & Marchioli 2001).

If we characterize all the coherent structures present in the area with the same $|\boldsymbol{\Omega}|$ isosurface but with both signs, a secondary, but relevant, item in this picture appears as a red isosurface identifying a smaller counter-rotating quasi-streamwise vortex of negative ω_x vorticity, centred at $z^+ = 9$ and extending well into the viscous wall layer. The presence of such small vortices was also demonstrated by Brooke & Hanratty (1993), who found that each turbulence-producing quasi-streamwise vortex in the viscous wall region is created in the downwash of another flow-oriented vortex. Brooke & Hanratty (1993) proposed a turbulence regeneration cycle in which each mature quasi-streamwise vortex, *parent vortex* (the green vortex in figure 9*a*), produces a small quasi-streamwise vortex of opposite sign, *offspring vortex*. Following other interpretations, the offspring vortices may be interpreted as the rear, wall-touching end of a counter-rotating quasi-streamwise vortex farther downstream (Schoppa & Hussain 1996, 1997).

It is not our object here to focus on the turbulence regeneration cycle. However, we aim at verifying and quantifying the action of the offspring vortices in trapping the particles in the wall layer. From figure 9(*a*), it is apparent that particles which enter the field of the offspring vortex may not easily escape and fall under the influence of the ejection maintained by the mature vortex. We verified whether the situation just described has statistical relevance and used a visual criterion to determine whether the structure dynamics shown in figure 9(*a*) is statistically more probable than others. We examined 50 flow fields spaced over time in order to have a large set of uncorrelated realizations. We observed an average sample of about 50 vortices taken from the same instantaneous flow field realization and we found single flow-oriented mature vortices coupled with secondary counter-rotating newly born vortices in more than 70% of the observations. Occasionally, this coupling is not present. We detected pairs of quasi-streamwise vortices with equal strength – i.e. characterizing the legs of the so-called *horseshoe vortices* (Zhou *et al.* 1999; Choi 2001) – in just 25% of the observations. Our observations agree well with previous results (Schoppa & Hussain 1996, 1997), in which it was pointed out that quasi-streamwise vortices preferably line up to flank the low-speed streaks as a staggered array.

We followed the evolution in time of the structures in figure 9(*a*): figure 9(*b*) shows the same box of figure 9(*a*) approximately 30 wall time units later and 150 wall units downstream. We followed the evolution of the newly born vortex with a convection velocity equal to $0.5U_C$, which corresponds to the $z^+ = 10$ location of the newly born

vortex. The parent vortex previously shown is no longer visible whereas the pocket of negative ω_x has grown both in length and width and has lifted from the wall. Under the cusp of the lifted low-speed streak, the green $\boldsymbol{\Omega}$ isosurface indicates the presence of a patch of positive ω_x vorticity, that will later become a third-generation vortex (Brooke & Hanratty 1993). Colours and symbols in figure 9(*b*) have the same meaning as in figure 9(*a*). The clockwise-rotating vortex on the left, pertaining to the influence area of the low-speed streak on the left of the figure, is not discussed in this context.

As is apparent from figure 9, the role of the secondary vortex is crucial in preventing particles from being entrained into the outer flow. As discussed in the previous section, energetic, strongly coherent ejections correlate well with particle fluxes away from the wall. In turn, strongly coherent ejections are generated by strong, mature vortices, which at the same time, are associated with offspring vortices. The combined action of the newly born vortex and the mature vortex is such as to reduce the width of the 'ejection avenue' through which particles in the wall layer have to pass to reach the outer flow.

Particles with $|w_P| < 10^{-3}$ (open circles) in figure 9(*b*) are mostly settled under the low-speed streak, in a wall layer confined between the offspring vortex and the wall. These *trapped* particles were pushed toward the wall by previous downsweeps but no ejection has yet occurred that is sufficiently energetic to re-entrain them. This behaviour is probably due to the above mechanism for near-wall vortex regeneration. The birth of new vortices is associated with strong spanwise motions which counteract the wall-normal pull due to local turbulence gradients or fluid ejections and prevent some particles from being re-entrained. The overall effect is to concentrate and keep particles within the sediment layer in elongated streaks that may be viewed as low-stress regions associated with a stagnation flow.

It is important now to underline the timing of the different events contributing to bring and segregate particles in the wall layer. The low-speed streaks, under which particles are accumulated, are long-lived wall structures. The time duration of quasi-streamwise vortices is much shorter. Strongly coherent sweeps, capable of driving particles toward the wall, and ejections strong enough to drive particles away from the wall are generated simultaneously by the forward end of the quasi-streamwise vortex. As observed in previous works (De Angelis *et al.* 1997), the frequency of ejections is about $80t^+$ and, as observed also by Niño & García (1996), it is the only way for a particle to be driven away from the wall layer (see the previous section). Thus, when a mature quasi-streamwise vortex generates a strongly coherent sweep, it simultaneously generates a strongly coherent ejection. However, the simultaneous presence of the newly born vortex – or rear end of a counter-rotating streamwise vortex farther downstream – prevents a large fraction of the particles from accessing the ejection area. Thus, the newly born vortex acts to enhance the energy level required to carry particles in the outer flow region and plays a primary role in reducing overall particle mixing.

A Lagrangian description of the local trajectory of particles when under the influence of the structures just described may help to elucidate further the particle trapping mechanisms. In figure 10(*a*), we show the mature vortex and the offspring vortex at the same time-step as figure 9(*a*), together with the trajectory of a number of particles. We chose several particles in interesting positions, i.e. trapped or ejected away from the wall layer, and we tracked their trajectory backward and forward. The dot-to-dot distance on a particle trajectory is $\Delta t^+ = 0.7065$ in wall time units. During this time, we can hypothesize that turbulence structures change slightly,

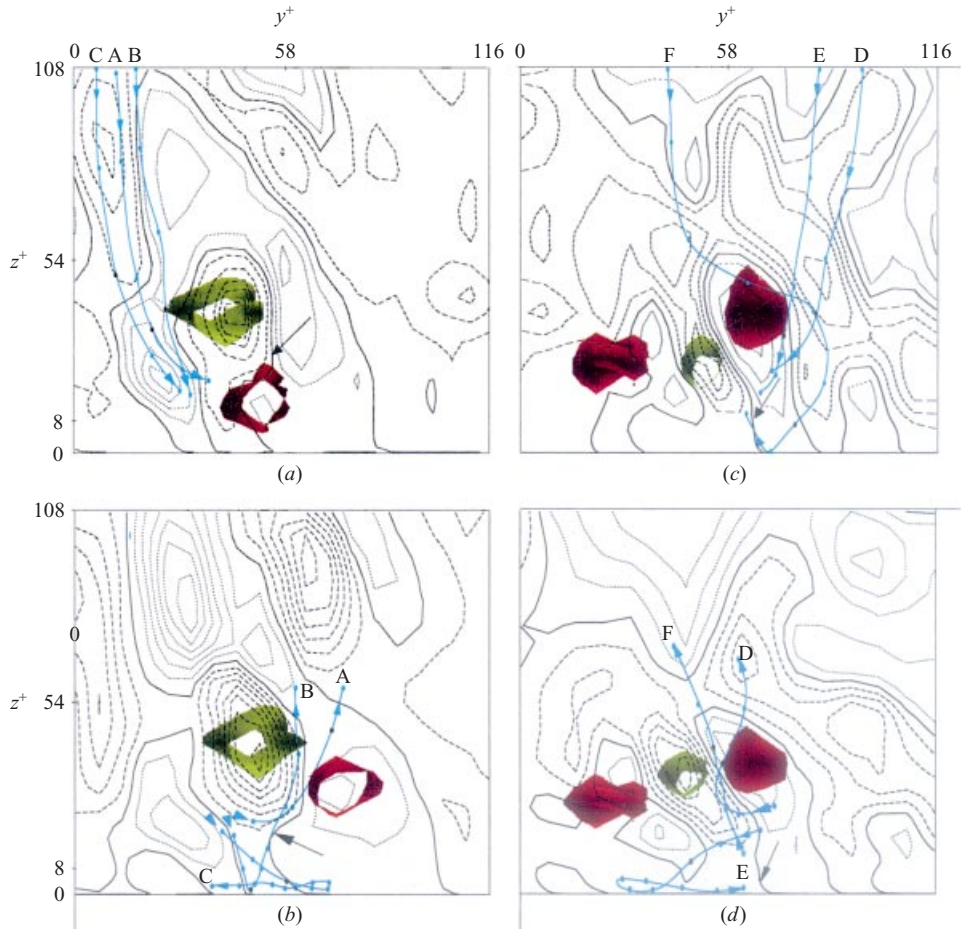

FIGURE 10. Near-wall turbulent structures with superimposed streamlines of channel flow at different times of the simulation: (*a*) $t^+ = 1412$, (*b*) $t^+ = 1414.8$, (*c*) $t^+ = 1450$, (*d*) $t^+ = 1452.8$. Dashed lines represent streamlines with positive values of the stream function ($\Psi > 0$), dotted lines represent streamlines with negative values of Ψ. Streamlines with $\Psi = 0$ are plotted as solid lines. Sample trajectories of few particles approaching the wall (labelled with letters A to F) are also plotted to show the influence of counter-rotating vortices on particle dynamics at the wall. Black dots on sample trajectories indicate the particle position at the same time step at which the flow structures are visualized. Particle positions are tracked backward and forward around this time step – dot-to-dot time is 0.7065.

their average life being more than 100 wall time units (Brooke & Hanratty 1993; Schoppa & Hussain 1997, 2000). In this figure, we also show the instantaneous flow streamlines calculated at the same time at which we visualized the quasi-streamwise vortices. Positive values for the stream function Ψ (dashed lines) are associated with counterclockwise-rotating vortices whereas negative values of Ψ (dotted lines) are associated with clockwise-rotating vortices. Streamlines with $\Psi = 0$ are plotted as solid lines. Consider the three particles labelled A, B and C in figure 10(*a*): their position at the time of the figure is identified by the black dot. Tracking their trajectory backward, we observe that the three particles left from the same fluid environment and, tracking their trajectory forward, we see that they end up in the same neighbourhood. However, and this is important for their future destiny, they

have different trajectory curvatures. Going now to figure 10(*b*), we can see the wall structure 2.8 wall time units later, approximately 11 wall units downstream. After this short time, the large vortex has changed slightly, and the smaller vortex has moved farther from the wall. The position of the three particles is again identified by the black dot. We shall now consider the overall trajectory of the three particles: the particle labelled A follows a neat path around the mature quasi-streamwise vortex in green, and after being swept toward the wall, enters the outer flow driven by the ejection. The particle labelled B follows a path similar to that of particle A but, before being entrained by the ejection, it bounces elastically off the wall. Particle C goes under the offspring vortex, very close to the wall, where it finds an adverse flow which pushes it backward parallel to the wall. This particle will be confined longer in the viscous wall layer.

In figure 10(*c*), we examine a similar situation generated by the clockwise-rotating quasi-streamwise vortex in red, with all symbols and positioning of letters maintaining the same meaning. Again, we chose three particles with different destinies. Particle D, after being entrained by the sweep, is able to pass between the mature vortex and the offspring vortex, along the black streamline – $\Psi = 0$ – which identifies the only escape route from the wall region. Particle E is driven too far under the offspring vortex and is not able to escape from the wall region. Particle F bounces off the wall and is able to follow the ejection to the outer flow.

If we now consider the streamlines patterns in figure 10, the action of the offspring vortex in trapping the particles in the wall layer is evident. The flow regions bordering the $\Psi = 0$ streamlines, indicated with the black arrows in figure 10, are source flows from the wall region. The presence of the offspring vortex associated with the effects of the mature vortex contributes to squeeze these regions – increasing contour density – thus reducing the probability for a particle to be entrained into the outer flow.

The aim of this section was to elucidate the mechanisms by which inertial particles are trapped in the near-wall region by the synchronicity among the turbulent transfer mechanisms, namely strongly coherent sweeps and ejections, and the regeneration cycle of the quasi-streamwise vortices. To this end, we focused on the smaller particles in our set ($\tau_P^+ = 3.8$), which show the higher tendency to respond to the trapping mechanism we are discussing.

A sample analysis conducted for the larger particle cases gave similar results from a qualitative viewpoint, indicating that, for the particle time scales investigated interacting with the wall structures characteristic of a channel flow at $Re_\tau = 150$, particles segregation mechanisms are similar. Quantitative figures relative to the different particles are different due to the different particle inertia, as previously pointed out in §§ 3.2, 3.3 and 3.4.

If, as in Adrian *et al.* (2000), we employ the term hairpin vortex to represent the broad class of quasi-streamwise structures which may be or may be not associated with a counter-rotating parallel vortex by a head of spanwise vorticity, the mechanism we propose for particle transfer in the region very near to the wall is consistent with Robinson's (1991) observations that the quasi-streamwise hairpin vortex legs dominate the buffer layer, whereas inclined necks and heads predominate in the logarithmic layer.

Furthermore, our mechanisms for particle transfer and trapping are also consistent with other experimental observations. Niño & García (1996) and García *et al.* (1996) observed that particle re-entrainment is most effectively performed by intense bursts of wall fluid occurring almost in correspondence with typical shear layers travelling at a convection velocity of about 0.70 to 0.80 of the local mean velocity. Similar

shear layers have been characterized by Adrian *et al.* (2000) in the framework of the hairpin-packet mechanism for the turbulence regeneration cycle. The hairpin packets travel at different convection velocities, enclose a low-velocity fluid region characterized by a series of Q2 events, and also enclose internal shear layers travelling at a velocity of $0.8U_\infty$ where U_∞ is the free-stream velocity. In a recent paper, Schoppa & Hussain (2002) gave an explanation for the formation of these shear layers and observed that [...] 'where a streamwise vortex [...] is formed on one flank of a streak, an internal shear layer forms on the other flank of the streaks'. The same authors (Schoppa & Hussain 1997, 2000), analysing turbulence structures in a minimal channel flow, ascribe to the low-speed streak lateral instability the responsibility for quasi-streamwise vortices regeneration. In particular, they observe that low-speed streaks go through quiescent phases – vortex-less low-speed streaks – and through active phases during which the low-speed streak surface bulges outward, taking a cusp-like shape, and coherent regions of streamwise vorticity roughly centred about 30 wall units far from the wall appear flanking the low-speed streak (see figure 2 in Schoppa & Hussain 2000, and figure 10 in Soldati & Marchioli 2001). These regions of streamwise vorticity are the signature of the forward-end of quasi-streamwise vortices, which are strong enough to generate strong ejections able to re-entrain particles in the outer flow. In figure 9(*a*), the low-speed streak is just going through one of these active phases and has the characteristic cusp-like shape flanked by a counter-clockwise rotating quasi-streamwise vortex which, in turn, is generating a strong ejection of wall fluid.

Our findings appear to support previous observations on particle re-entrainment mechanisms by proving the efficiency of the strongly coherent ejections. Yet, they add information, since strongly coherent ejections are extremely effective in transferring particles from the wall region to the outer flow provided that particles are not prevented from reaching the region where ejections can entrain them.

4. Conclusions

The identification of the mechanisms leading to particle transfer in the wall region and to particle segregation in the viscous sublayer in regions where the streamwise fluid velocity is lower than the mean is of fundamental significance for a number of technological and environmental applications. A sound understanding of these mechanisms requires analysis of the interactions between the coherent structures controlling the turbulent transfer at the wall and particle dynamics.

In this work, we examined the dynamics of large numbers of heavy particles – flyashes in air – dispersed in a vertical upward channel flow. The particle to fluid density ratio was 769.23 and particle size was $d_P = 40\,\mu\text{m}$, $d_P = 110\,\mu\text{m}$ and $d_P = 220\,\mu\text{m}$ in the three cases investigated. The fluid was driven by a pressure gradient and the shear Reynolds number was $Re_\tau = 150$ which, for a channel 4 cm wide, gave an average velocity of $1.65\,\text{m}\,\text{s}^{-1}$. We had two objects in this research: the first was to identify and quantify the turbulent convective mechanisms which transfer particles toward the wall and toward the outer flow. The second was to determine why particle transfer toward the wall is more efficient than particle transfer away from the wall.

Since our aim was to examine the influence of turbulence structures on particle behaviour, we did not consider feedback of particles on the flow field. As demonstrated in the experiments by Kaftori *et al.* (1995*a*, *b*), turbulence characteristics change only slightly for dilute dispersions, thus permitting us to obtain results with general relevance.

First, we examined the relationship between particle fluxes in and out the wall layer and momentum fluxes at the wall. We found that a strong correlation exists between sweep events – i.e. coherent downwash of outer fluid to the wall – and particle flux toward the wall, and between ejection events – i.e. coherent upwash of wall fluid toward the outer flow – and particle flux toward the outer flow. This correlation is almost perfect for smaller particles and a little weaker for larger particles. We found that particles are transferred almost exclusively by strongly coherent sweeps and ejections.

We also tried to quantify the efficiency of these coherent local convective motions, calculating the probability that a particle will go toward the wall or away from the wall conditioned by the presence of a sweep or an ejection. We found that sweeps and ejections are extremely efficient for transferring small particles of $\tau_P^+ = 3.8$. In other words, if a small particle travels toward the wall, it is engulfed in a sweep whereas if the particle travels away from the wall, it is driven by an ejection. For larger particles, $\tau_P^+ = 116.3$, we found that most of the particles are still transferred by sweeps and ejections but a higher proportion of particles with positive wall-normal velocity appears in fluid environments characterized by negative wall-normal velocity, and vice versa. In particular, for the larger set of particles, the fraction of particles travelling toward the wall in a non-sweep environment is smaller than the fraction of particles travelling away from the wall in a non-ejection environment.

A possible explanation is to be found in the ratio of particle time scale to fluid structure time scale. The characteristic time scale of turbulent structures decreases progressively as the structures get closer to the wall. Larger particles have a larger time scale and filter out the effects of the smaller fluid scales. Thus, the larger momentum gained by the large particles through the interactions with the large scales in the buffer layer which are able to drive particles to the wall may be sufficient to let the particle bounce elastically off the wall toward the outer flow, crossing the smaller-scale structures in the vicinity of the wall, which are unable to further modify the particle trajectory.

Having established quantitatively the action of the instantaneous realizations of the Reynolds stress on particle transfer, our object was then to determine why a large fraction of the particles entering the wall region are unable to escape and remain trapped in the low-streamwise-velocity environment. This phenomenon causes accumulation of particles in the near-wall region and when properly understood and characterized, can be of extreme interest for a number of applications, ranging from new gas cleaning devices and prediction of environmental sedimentation processes, to sizing and control of surface chemical reactions. Evidence of higher particle concentration in the proximity of the walls was observed previously (Caporaloni *et al.* 1975), and turbophoresis was the name given to it. From a statistical viewpoint, turbophoresis is the outcome of the combined effects of particle inertia and the effect of the wall on the distribution of turbulence moments. In practice, particles are convected down the gradients of turbulence intensity (Reeks 1983). The main purpose of this work was to establish a model for particle trapping at the wall based on the joint examination of particle dynamics together with the dynamics of the turbulence structures populating the near-wall region of the turbulent boundary layer.

From previous works (Schoppa & Hussain 1996, 1997, 2000; Jeong *et al.* 1997; Soldati & Marchioli 2001), it was possible to establish that: (i) low-speed streaks are long-lived structures, (ii) low-speed streaks are flanked by clockwise and counterclockwise-rotating quasi-streamwise vortices distributed mostly (in about 75%

of the cases) as a staggered array, (iii) quasi-streamwise vortices generate strongly coherent sweeps and ejections. In this work, we were able to verify that (iv) particles are driven toward the wall and toward the outer flow only by the strongly coherent sweeps and ejections. Thus, examining in detail the dynamics of the wall structures in connection with the dynamics of the particles entering and exiting the wall layer, we were able to appreciate fully the relevance of a secondary wall structure which was described by Brooke & Hanratty (1993) and by Bernard *et al.* (1993). In particular, we focus on the near-wall region of the turbulent boundary layer and we examined the role of the rear-end of a quasi-streamwise vortex that is very near to the wall in preventing particles in the proximity of the wall from being re-entrained by the pumping action of the large, farther from the wall, forward end of a following quasi-streamwise vortex. The local flow structure produced by this couple prevents a number of the particles that have entered the wall layer from being entrained toward the outer flow. In particular, even though the strongly coherent sweep events required to drive particles to the wall are associated with strongly coherent ejections capable of driving the particles toward the outer flow, the simultaneous presence of the offspring vortex acts as to reduce the width of the 'ejection channel'. In practice, only particles which enter the wall layer with a specific trajectory curvature may be able to be entrained back into the outer flow.

The intensity of particle fluxes is given by the efficiency of the transfer mechanisms combined with the availability of particles in the regions where the transfer mechanisms can entrain them. The reasons for turbophoresis now appear clear: it is the synchronicity between the strongly coherent ejections, which are able to entrain the particles, and the presence of the rear-end of a quasi-streamwise vortex very near to the wall which prevents equal in and out wall fluxes.

Our results confirm previous results on particle re-entrainment mechanisms and prove the efficiency of the strongly coherent ejections and sweeps as particle transfer mechanisms. However, we found evidence that strongly coherent ejections are extremely effective in transferring only those particles which are not prevented from reaching the region where ejections can entrain them.

The identification of these mechanisms which appear to control particle trapping at the wall is relevant for the future direction of mathematical modelling of wall-bounded particle-laden flows, including advection-diffusion-type field approaches (Slater & Young 2001; Young & Leeming 1997; Cerbelli *et al.* 2001) and Lagrangian approaches based on large-eddy simulations (Armenio, Piomelli & Fiorotto 1999). A final remark should be added at this point. In our work, particles behave independently of the other particles – no collisions. This assumption appears largely justified in the outer flow, where particle number density is low, yet it may not hold in the wall region, with large particle number density. For the particle size investigated in the present work, we believe that collisions may change quantitatively the phenomena we discussed. More significant changes may occur for larges particles (Squires & Simonin 2002).

The authors would like to thank Giorgio Michelazzo for performing some of the calculations and visualizations. Special thanks to Professor Guido Buresti for his insightful remarks. Financial support from MURST under Grant 9809326392_005 and from the Regional Authority of Friuli Venezia Giulia under the Grant *Fluidodinamica e Analisi delle Dispersioni nella Bassissima Atmosfera del Friuli Venezia Giulia* are gratefully acknowledged.

REFERENCES

Adrian, R. J., Meinhart, C. D. & Tomkins, C. D. 2000 Vortex organization in the outer region of the turbulent boundary layer. *J. Fluid Mech.* **422**, 1–54.

Armenio, V. & Fiorotto, V. 2001 The importance of the forces acting on particles in turbulent flows. *Phys. Fluids* **13**, 2437–2440.

Armenio, V., Piomelli, U. & Fiorotto, V. 1999 Effect of the subgrid scales on particle motion. *Phys. Fluids* **11**, 3030–3042.

Balachandar, S. & Maxey, M. R. 1989 Methods for evaluating fluid velocities in spectral simulations of turbulence. *J. Comput. Phys.* **83**, 96–125.

Bernard, P. S., Thomas, J. M. & Handler, R. A. 1993 Vortex dynamics and the production of Reynolds stress. *J. Fluid Mech.* **253**, 385–419.

Brooke, J. W. & Hanratty, T. J. 1993 Origin of turbulence-producing eddies in channel flow. *Phys. Fluids* A **5**, 1011–1022.

Brooke, J. W., Kontomaris, K., Hanratty, T. J. & McLaughlin, J. B. 1992 Turbulent deposition and trapping of aerosols at a wall. *Phys. Fluids* A **4**, 825–834.

Caporaloni, M., Tampieri, F., Trombetti, F. & Vittori, O. 1975 Transfer of particles in nonisotropic air turbulence. *J. Atmos. Sci.* **32**, 565–568.

Cerbelli, S., Giusti, A. & Soldati, S. 2001 ADE approach to predicting dispersion of heavy particles in wall bounded turbulence. *Intl J. Multiphase Flow* **27**, 1861–1879.

Choi, K.-S. 2001 Turbulent drag reduction mechanisms: strategies for turbulence management. In *Turbulence Modulation and Control* (ed. A. Soldati & R. Monti). CISM Courses and Lectures, vol. 415, pp. 161–211. Springer.

Chong, M. S., Perry, A. & Cantwell, B. J. 1990 A general classification of three-dimensional flow fields. *Phys. Fluids* A **2**, 765–777.

Cleaver, J. W. & Yates, B. 1975 A sub layer model for the deposition of particles from a turbulent flow. *Chem. Engng Sci.* **30**, 983–992.

Crowe, C. T., Chung, J. N. & Troutt, T. R. 1988 Particle mixing in free shear flows. *Prog. Energy Combust. Sci.* **14**, 171–194.

De Angelis, V., Lombardi, P., Andreussi, P. & Banerjee, S. 1997 Microphysics of scalar transfer at air–water interfaces. *IMA Conf. on Wind over Wave Couplings, Salford, UK, 8–10 April, 1997* (ed. S. G. Sajjadi, N. H. Thomas & J. C. R. Hunt). Oxford University Press.

Eaton, J. K. & Fessler, J. R. 1994 Preferential concentration of particles by turbulence. *Intl J. Multiphase Flow*, **20**, 169–209.

Friedlander, S. K. & Johnstone, H. F. 1957 Deposition of suspended particles from turbulent gas streams. *Ind. Engng Chem. Res.* **49**, 1151–1156.

García, M., Lopez, F. & Niño, Y. 1995 Characterization of near-bed coherent structures in turbulent open channel flow using synchronized high-speed video and hot-film measurements. *Exps. Fluids* **19**, 16–28.

García, M., Niño, Y. & López, F. 1996 Laboratory observations of particle entrainment into suspension by turbulent bursting. In *Coherent Flow Structures in Open Channels* (ed. P. J. Ashworth, S. J. Bennett, J. L. Best & S. J. McLelland), pp. 63–85. Wiley & Sons.

Guezennec, Y. G. & Choi, W. C. 1989 Stochastic estimation of coherent structures in turbulent boundary layers. In *Proc. Zoran P. Zaric Memorial International Seminar on Near Wall Turbulence, May 1988* (ed. S. J. Kline & N. H. Afghan), pp. 420–436. Hemisphere.

Guezennec, Y. G., Piomelli, U. & Kim, J. 1989 On the shape and dynamics of wall structures in turbulent channel flow. *Phys. Fluids* A **1**, 764–766.

van Haarlem, B., Boersma, B. J. & Nieuwstadt, F. T. M. 1998 Direct numerical simulation of particle deposition onto a free-slip and no-slip surface. *Phys. Fluids* **10**, 2608–2620.

Jimenez, J., Moin, P., Moser, R. & Keefe, L. 1988 Ejection mechanisms in the sublayer of a turbulent channel. *Phys. Fluids* **31**, 1311–1313.

Jimenez, J. & Pinelli, A. 1999 The autonomous cycle of near-wall turbulence. *J. Fluid Mech.* **389**, 335–359.

Jeong, J. & Hussain, F. 1995 On the identification of a vortex. *J. Fluid Mech.* **285**, 69–83.

Jeong, J., Hussain, F., Schoppa, W. & Kim, J. 1997 Coherent structures near the wall in a turbulent channel flow. *J. Fluid Mech.* **332**, 185–214.

Kaftori, D., Hetsroni, G. & Banerjee, S. 1995*a* Particle behavior in the turbulent boundary layer. I. Motion, deposition, and entrainment. *Phys. Fluids* **7**, 1095–1106.

Kaftori, D., Hetsroni, G. & Banerjee, S. 1995*b* Particle behavior in the turbulent boundary layer. II. Velocity and distribution profiles. *Phys. Fluids* **7**, 1107–1121.

Kallio, G. A. & Reeks, M. W. 1989 A numerical simulation of particle deposition in turbulent boundary layers. *Intl J. Multiphase Flow* **15**, 433–446.

Kim, J., Moin, P. & Moser, R. 1987 Turbulence statistics in fully developed channel flow at low Reynolds number. *J. Fluid Mech.* **177**, 133–166.

Kline, S. J., Reynolds, W. C., Schraub, F. A. & Runstadler, P. W. 1967 The structure of turbulent boundary layers. *J. Fluid Mech.* **30**, 741–773.

Kontomaris, K., Hanratty, T. J. & McLaughlin, J. B. 1992 An algorithm for tracking fluid particles in a spectral simulation of turbulent channel flow. *J. Comput. Phys.* **103**, 231–242.

Kulick, J. D., Fessler, J. R. & Eaton, J. K. 1994 Particle response and turbulence modification in fully developed channel flow. *J. Fluid Mech.* **277**, 109–134.

Lam, K. & Banerjee, S. 1992 On the condition of streak formation in bounded flows. *Phys. Fluids* A **4**, 306–320.

Lombardi, P., De Angelis, V. & Banerjee, S. 1996 Direct numerical simulation of near-interface turbulence in coupled gas–liquid flow. *Phys. Fluids* **8**, 1643–1665.

Lu, D. M. & Hetsroni, G. 1995 Direct numerical simulation of a turbulent channel flow with heat transfer. *Intl J. Heat Mass Transfer*, **38**, 3241–3251.

Lyons, S. L., Hanratty, T. J. & McLaughlin, J. B. 1991 Large-scale computer simulation of fully developed turbulent channel flow with heat transfer. *Intl J. Numer. Meth. Fluids* **13**, 999–1028.

McLaughlin, J. B. 1989 Aerosol particle deposition in numerically simulated channel flow. *Phys. Fluids* **1**, 1211–1224.

McLaughlin, J. B. 1991 Inertial migration of a small sphere in linear shear flows. *J. Fluid Mech.* **224**, 261–274.

Niño, Y. & Garcia, M. H. 1996 Experiments on particle–turbulence interactions in the near-wall region of an open channel flow: implications for sediment transport. *J. Fluid Mech.* **326**, 285–319.

Orlandi, P. & Jimenez, J. 1994 On the generation of turbulent wall friction. *Phys. Fluids* **6**, 634–641.

Ounis, H., Ahmadi, G. & McLaughlin, J. B. 1993 Brownian particle deposition in a directly simulated channel flow. *Phys. Fluids* **5**, 1427–1432.

Pan, Y. & Banerjee, S. 1996 Numerical simulation of particle interactions with wall turbulence. *Phys. Fluids* **8**, 2733–2755.

Pedinotti, S., Mariotti, G. & Banerjee, S. 1992 Direct numerical simulation of particle behavior in the wall region of turbulent flow in horizontal channels. *Intl J. Multiphase Flow*, **18**, 927–941.

Perry, A. & Chong, M. S. 1987 A description of eddying motions and flow patterns using critical point concepts. *Annu. Rev. Fluid Mech.* **9**, 125–148.

Reeks, M. W. 1983 The transport of discrete particles in inhomogeneous turbulence. *J. Aerosol Sci.* **14**, 729–739.

Rizk, M. A. & Elghobashi, S. E. 1985 The motion of a spherical particle suspended in a turbulent flow near a plane wall. *Phys. Fluids* **28**, 806–817.

Robinson, S. K. 1991 Coherent motions in the turbulent boundary layer. *Annu. Rev Fluid Mech.* **23**, 601–639.

Rouson, D. W. I. & Eaton, J. K. 2001 On the preferential concentration of solid particles in turbulent channel flow. *J. Fluid Mech.* **428**, 149–169.

Saffman, P. G. 1965 The lift on a small sphere in a slow shear flow. *J. Fluid Mech.* **22**, 385–400; and Corrigendum **31** (1968), 624.

Schoppa, W. & Hussain, F. 1996 New aspects of vortex dynamics relevant to coherent structures in turbulent flows. In *Eddy Structure Identification* (ed. J. P. Bonnet). CISM Courses and Lectures, vol. 353, pp. 61–143. Springer.

Schoppa, W. & Hussain, F. 1997 Genesis and dynamics of coherent structures in near-wall turbulence. In *Self-sustaining Mechanisms of Wall Turbulence* (ed. R. Panton). Advances in Fluid Mechanics, vol. 15, pp. 385–422. Computational Mechanics Publications.

Schoppa, W. & Hussain, F. 2000 Coherent structure dynamics in near-wall turbulence. *J. Fluid Dyn. Res.* **26**, 119–139.

Schoppa, W. & Hussain, F. 2002 Coherent structure generation in near-wall turbulence. *J. Fluid Mech.* **453**, 57–108.

Slater, S. A. & Young, J. B. 2001 The calculation of inertial particle transport in dilute gas–particle flows. *Intl J. Multiphase Flow* **27**, 61–87.

Soldati, A. 2002 Influence of large-scale streamwise vortical EHD flows on wall turbulence. *Intl J. Heat Fluid Flow* **23**, 441–443.

Soldati, A. & Banerjee, S. 1998 Turbulence modification by large scale organized electrohydrodynamic flows. *Phys. Fluids* **10**, 1742–1756.

Soldati, A., Casal, M., Andreussi, P. & Banerjee, S. 1997 Lagrangian simulation of turbulent particle dispersion in Electrostatic Precipitators. *AIChE J.* **43**, 1403–1413.

Soldati, A. & Marchioli, C. 2001 Prospects for modulation of turbulent boundary layer by EHD flows. In *Turbulence Structure and Modulation* (ed. A. Soldati & R. Monti). CISM Courses and Lectures, vol. 415, pp. 119–160. Springer.

Squires, K. D. & Simonin, O. 2002 Applications of DNS and LES to dispersed two-phase turbulent flow. In Proc. 10th *Workshop on Two-phase Flow Predictions, Merseburg, DE, April 9–12, 2002* (ed. M. Sommerfeld), pp. 152–163.

Sun, Y. F. & Lin, S. P. 1986 Aerosol concentration in a turbulent flow. *J. Colloid Interface Sci.* **113**, 315–320.

Tchen, C. M. 1947 Mean value and correlation problems connected with the motion of small particles suspended in a turbulent fluid. PhD Thesis, Delft.

Uijttewaal, W. S. J. & Oliemans, R. V. A. 1996 Particle dispersion and deposition in direct numerical and large eddy simulations of vertical pipe flows. *Phys. Fluids* **8**, 2590–2604.

Urushihara, T., Meinhart, C. D. & Adrian, R. J. 1993 Investigation of the logarithmic layer in pipe flow using Particle Image Velocimetry. In *Near Wall Turbulent Flows* (ed. R. M. So, C. G. Speziale & B. E. Launder), pp. 433–446. Elsevier.

Wallace, J. M., Eckelmann, H., Brodkey, R. S. 1972 The wall region in turbulent shear flow. *J. Fluid Mech.* **54**, 39–48.

Wang, Q. & Squires, K. D. 1996 Large eddy simulation of particle deposition in a vertical turbulent channel flow. *Intl J. Multiphase Flow* **22**, 667–683.

Wei Ling, Chung, J. N., Troutt, T. R. & Crowe, C. T. 1998 Direct numerical simulation of a three-dimensional temporal mixing layer with particle dispersion. *J. Fluid Mech.* **358**, 61–85.

Wells, M. R. & Stock, D. E. 1983 The effect of crossing trajectories on the dispersion of particles in turbulent flow. *J. Fluid Mech.* **136**, 31–62.

Willmarth, W. W. & Lu, S. S. 1972 Structure of the Reynolds stress near the wall. *J. Fluid Mech.* **55**, 65–92.

Yeung, P. K. & Pope, S. B. 1988 An algorithm for tracking fluid particles in numerical simulations of homogeneous turbulence. *J. Comput. Phys.* **79**, 373–416.

Young, J. & Leeming, A. 1997 A theory of particle deposition in a turbulent pipe flow. *J. Fluid Mech.* **340**, 129–159.

Zhang, H. & Ahmadi, G. 2000 Aerosol particle transport and deposition in vertical and horizontal turbulent duct flows. *J. Fluid Mech.* **406**, 55–80.

Zhou, J., Adrian, R. J., Balachandar, S. & Kendall, T. M. 1999 Mechanisms for generating coherent packets of hairpin vortices in channel flow. *J. Fluid Mech.* **387**, 353–396.